



HAL
open science

Saponite-anthocyanin pigments: Slipping between the sheets

Luciano Clécio Brandão Lima, Fabrícia Castro-Silva, Edson Cavalcanti Silva-Filho, Maria Gardennia Fonseca, Maguy Jaber

► **To cite this version:**

Luciano Clécio Brandão Lima, Fabrícia Castro-Silva, Edson Cavalcanti Silva-Filho, Maria Gardennia Fonseca, Maguy Jaber. Saponite-anthocyanin pigments: Slipping between the sheets. *Microporous and Mesoporous Materials*, 2020, 300, pp.110148. 10.1016/j.micromeso.2020.110148 . hal-02887318

HAL Id: hal-02887318

<https://hal.sorbonne-universite.fr/hal-02887318v1>

Submitted on 2 Jul 2020

HAL is a multi-disciplinary open access archive for the deposit and dissemination of scientific research documents, whether they are published or not. The documents may come from teaching and research institutions in France or abroad, or from public or private research centers.

L'archive ouverte pluridisciplinaire **HAL**, est destinée au dépôt et à la diffusion de documents scientifiques de niveau recherche, publiés ou non, émanant des établissements d'enseignement et de recherche français ou étrangers, des laboratoires publics ou privés.

1 **Saponite-anthocyanin pigments: slipping between the sheets**

2

3

4 **Luciano Clécio Brandão Lima^{1,2}, Fabrícia Castro-Silva^{1,2}, Edson Cavalcanti Silva-**
5 **Filho¹, Maria Gardênnia Fonseca³, Maguy Jaber^{2*}**

6

7

8 ¹LIMAV, Univ. Federal do Piauí – UFPI, 64049-550 Piauí, Brazil

9

²Sorbonne Université, CNRS UMR 8220, LAMS, Institut Universitaire de France

10

(IUF), case courrier 225, 4 pl. Jussieu 75252 Paris cedex 05, France

11

³NPE-LACOM, Univ. Federal da Paraíba – UFPB, João Pessoa, 58051-900 Paraíba,

12

Brazil

13

14 **ABSTRACT**

15

16 The present work describes the synthesis and characterization of hybrid
17 materials based on β -cyclodextrin (β -CD) and cetyltrimethylammonium bromide
18 (CTAB) intercalated into saponite (SAP) and a commercially available powder of
19 anthocyanin dye, Crystal Red Grape (RG). The interactions between the organic dye
20 guest and the organo-clay host were investigated by X-ray diffraction,
21 thermogravimetric analysis, transmission electronic microscopy and ^{13}C solid state
22 nuclear magnetic resonance. The results support complex formation between β -CD and
23 CTAB, their intercalation into the clay interlayer spaces or surface loading, and their
24 interaction with RG (CTAB_SAP-RG, β -CD_SAP-RG and β -CD+CTAB_SAP-RG).
25 The hybrid pigments formed exhibit different colors, enhanced stability against visible
26 light irradiation and basic pH conditions. These hybrid pigments are environmentally
27 friendly and can be promising candidates in different application fields.

28

29 **KEYWORDS:** Saponite, Natural dye, Adsorption, Hybrid pigment, Color change.

30

31 **1. Introduction**

32

33 The whole spectrum of colors obtained from natural sources has been employed
34 and improved since the ancient civilization, but their use declined during the
35 development of organic chemistry in 19th century, with the “boom” of synthetic dyes
36 and pigments to get away from the limitations of natural dyes, which are subject to the
37 growing seasons of the plants or the life-cycles of the insects [1,2].

38 This context has lead the researches into natural dyes to take main focus to
39 historical, archaeological and cultural heritage aspects. However, in the last few
40 decades, the efforts of producing dyes providing long-lasting coloring effect comes at
41 the cost of complex organic structures and hazardous effects, reviving the age-old quest
42 of humankind for natural resources, since the conventional uses of synthetic dyes have
43 posed serious threat to global environment. In this way, the demand for eco-friendly
44 products is switching the trend of using synthetic dyes over the use of naturally
45 occurring colorants [3,4].

46 The anthocyanins are the natural pigments that humanity and animals have most
47 consumed from the beginning of time. Anthocyanins are therefore a highly desirable
48 substitute for synthetic food colors, being regarded to be non-toxic and strongly
49 associated to the disease prevention activities found in their sources by opposition to the
50 synthetic food pigments [5–7].

51 Anthocyanins are responsible for almost all nuances of blue, red, or purple
52 pigments found in plants, especially flowers, fruits, and tubers. They are water-soluble
53 glycosylated polyhydroxy and polymethoxy derivatives of 2-phenylbenzopyrylium
54 (flavylium) salts that have a common C₆—C₃—C₆ structure consisting of two aromatic
55 rings linked through an oxygenated heterocycle [8,9]. These molecules have an
56 antioxidant and free-radical scavenging properties which promote their recognized anti-
57 inflammatory, antitumor, anti-mutagenic, antiulcer, antiangiogenic, and antiaging
58 activities in addition to its diabetes prevention.

59 Despite their use in several fields due to their mentioned properties,
60 anthocyanins have limitations due to their photo- and chemical-stabilities [10].
61 Anthocyanin dyes are unstable at external environmental conditions such as light, pH,
62 oxygen, temperature [11].

63 Therefore, biohybrid compounds that combine these biomolecules and an
64 inorganic counterpart such as clay minerals have been widely investigated to reverse

65 these limitations by complexation in the host materials [12–14]. This field of research
66 has grown from studies about the first and most famous example of biohybrid, Maya
67 blue, which is composed of a natural clay mineral (palygorskite) and indigo dye of
68 biological origin [1,15,16].

69 The strategy to achieve the same stability known to Maya blue has been leading
70 the scientists to try to enhance other organic dyes for several applications. Concerning
71 the studies about anthocyanins, montmorillonite has been investigated as inorganic host
72 materials in recent years [12,17,18], followed by palygorskite [19,20], sepiolite [21],
73 laponite [22] and saponite [23]. However, no study explored the stability enhancement
74 for anthocyanin after adsorption on modified clay.

75 Among the many different types of clay minerals, saponite is a 2:1 trioctahedral
76 phyllosilicate belonging to smectite group, which shows interesting properties due to
77 their intercalation/exfoliation characteristics, large specific surface area, surface acidity,
78 cation exchange capacity, thermal stability, biocompatible, and non-toxic properties
79 [24].

80 The structure of saponite is composed of a magnesium octahedral sheet
81 sandwiched between two silicon tetrahedral sheets via sharing oxygen. Substitution of
82 Si^{4+} cations by Al^{3+} cations in the tetrahedral layer confers a negative charge generally
83 compensated by alkaline or alkaline earth cations located in the interlayer space. The
84 general formula of saponite can be expressed as $\text{M}^+_x[\text{Si}_{4-x}\text{Al}_x][\text{Mg}_3\text{O}_{10}(\text{OH})_2 \cdot n\text{H}_2\text{O}$,
85 where M is the exchangeable interlayer cation, x ($0.2 \leq x \leq 1.2$) is the fraction of
86 aluminum present in Si-O tetrahedral sheets, and n is the number of water molecules
87 [25,26].

88 Due to its negatively charged surface, saponite can be modified through the
89 replacement of the interlayer inorganic cations by organic ones. Structures with organic
90 cations, for example with quaternary ammonium cations such as
91 hexadecyltrimethylammonium bromide (CTAB), have been extensively studied to
92 provide surfactant-modified clays which can acquire hydrophobic and organophilic
93 characteristics via the interlayer exchange process. The characteristics of this composite
94 make it a promising candidate for the incorporation of dyes and aromatic compounds
95 [13,27–30].

96 Moreover, surface modification of clay minerals with biopolymers such as
97 starch, cellulose, chitosan and cyclodextrin was also reported for several applications
98 [31–34]. It can be noticed that the interaction between polysaccharides and

99 anthocyanins has shown to be especially important to improve the stability of the latter
100 [35,36]. Among the wide range of biopolymers, **cyclodextrin** has gained prominence
101 due to its ability to form non-covalent inclusion complexes due to the adaptable
102 hydrophobic tridimensional cavity. **Cyclodextrin** (CDs) are cyclic D-glucopyranose
103 oligomers, which the most common are known to have six, seven, or eight glucose units
104 linked by 1,4- α -glucosidic bonds, termed as α -, β -, and γ -CDs, respectively [37,38].

105 In this work, we report on the synthesis and characterization of hybrid pigments
106 based on saponite, as well as its equivalent modified with β -cyclodextrin (β -CD) and
107 **hexadecyltrimethylammonium** bromide (CTAB), and a commercially available
108 powdered anthocyanin dye, Crystal Red Grape (RG). The interactions and structural
109 characterizations were also carried out by different techniques to study the chemical-
110 and photo-stabilities of the obtained pigments.

111

112 **2. Materials and methods**

113 **2.1. Materials**

114

115 Anthocyanin source was a Crystal Red Grape (RG) donated by San Joaquin
116 Valley Concentrates (Fresno, CA, USA). Hexadecyltrimethylammonium bromide
117 (CTAB), β -cyclodextrin (β -CD), citric acid, sodium citrate, sodium hydroxide,
118 hydrochloric acid, and other applied chemicals were purchased from Aldrich or Sigma-
119 Aldrich, all with an analytical grade and used without any previous purification.

120 **2.2. Saponite synthesis**

121

122 For the synthesis of sodium saponite, the reagents were mixed in the following
123 order according to the following theoretical formula: $\text{Na}_{0.3}(\text{Si}_{3.7}\text{Al}_{0.3})\text{Mg}_3\text{O}_{10}(\text{OH})_2$:
124 deionized water, hydrofluoric acid (40%, wt), sodium acetate (99%, wt), magnesium
125 acetate tetrahydrate (99%, wt), basic aluminum acetate (19%, wt) and silica (Aerosil
126 130). The resulted hydrogels were aged under stirring at room temperature for 2 h and
127 then were autoclaved at 300 °C, 90 bars for 6 h. The autoclaves were cooled to room
128 temperature and the products were washed thoroughly with distilled water and
129 centrifuged. The solids were then dried at 50 °C for 24 h [26].

130

131 **2.3. **Synthesis** of inclusion complex β -CD+CTAB.**

132

133 The inclusion complex formed by reaction of β -CD with CTAB was prepared
134 according to a method previously described (Yei et al., 2005) with modifications.
135 Solutions of CTAB (5.59 mmol) and β -CD (16.8 mmol) in water (80 mL) were
136 prepared and mixed at room temperature. The mixture was stirred at 70 °C for 8 h and
137 then it was left to stand at room temperature overnight. The mixture became turbid and
138 the complex was obtained as a white crystalline precipitate. The precipitated product
139 was collected after centrifugation and dried at 70 °C. The complex was then washed
140 several times with water to remove any uncomplexed β -CD and CTAB. Finally, the
141 powder was dried at 60 °C for 24 h.

142

143 **2.4. Synthesis of hybrids organo-clay composites**

144

145 Following the method described in [39] with modifications, a suspension of
146 saponite (SAP, 5 g) in distilled water (250 mL) was stirred overnight in a 500 mL flask.
147 The organic molecules (β -CD, CTAB or β -CD+CTAB inclusion complex; 2 g) were
148 dissolved in 10 mL of 1 N HCl solution and added dropwise at room temperature to the
149 stirred aqueous solutions of SAP. After stirring the mixture for 3 h, the white precipitate
150 was collected by centrifugation, washed with water until no bromide ion could be
151 detected by an aqueous AgNO_3 solution, and then dried at 60 °C for 24 h. The O-SAP
152 materials obtained are named β -CD_SAP, CTAB_SAP and β -CD+CTAB_SAP.

153

154 **2.5. Adsorption studies**

155

156 Anthocyanin powder (RG) was dissolved in 0.020 mol·L⁻¹ citric acid buffer
157 solution (sodium citrate, citric acid at pH 3.0) to prepare a 5000 mg·L⁻¹ solution that
158 was used as stock solution.

159

160 **2.5.1 Effect of contact time on the adsorption**

161

162 The kinetics adsorption of anthocyanin on the materials were carried out as
163 follows: 20.0 mg of saponite (SAP) was added to 20.0 mL of 1000.0 mg·L⁻¹ dye
164 solution and reacted for a time range of 2-240 minutes under mechanical stirring at 150
165 rpm and 25 °C at pH 3. The samples were then centrifuged and equilibrium dye

166 concentrations were determined by UV-visible spectrophotometer (Model: Ocean
167 optics, HR2000) at 525 nm.

168 The quantity (moles) of the dye fixed in the adsorbate (q_e) was determined by
169 the Eq.(1),

$$170 \quad q_e = \frac{(C_o - C_e) * V}{m} \quad (1)$$

171 where C_0 and C_e are the initial and equilibrium concentrations in solution ($\text{mg}\cdot\text{L}^{-1}$),
172 m is the mass of the material in g and V is the volume of the solution used in mL.

173 Experimental results were adjusted to the pseudo-first [40], pseudo-second order
174 [41] and Elovich [42] adsorption kinetic models as described the following Eqs. (2)–
175 (4):

176

$$177 \quad \text{Pseudo-first order:} \quad \ln(q_{e,\text{exp}} - q_t) = \ln q_{e,\text{cal}} - K_1 t \quad (2)$$

$$178 \quad \text{Pseudo-second order:} \quad \frac{t}{q_t} = \frac{1}{K_2 q_{e,\text{cal}}^2} + \frac{1}{q_{e,\text{cal}}} t \quad (3)$$

$$179 \quad \text{Elovich:} \quad q_t = \beta(\ln \alpha \beta) + \beta(\ln t) \quad (4)$$

180 Where q_e and q_t $\text{mg}\cdot\text{g}^{-1}$ are the adsorption capacities at the equilibrium and in a
181 time t (min) respectively. In the Eq. (4) α ($\text{mg}\cdot\text{g}^{-1} \text{min}^{-1}$) and β ($\text{g}\cdot\text{mg}^{-1}$) are the initial
182 adsorption rates and Elovich constant related to the extent of surface coverage and also
183 to the activation energy involved in chemisorption, respectively.

184

185 **2.5.2 Effect of initial concentration on the adsorption**

186

187 To investigate the influence of anthocyanin concentration on adsorption, 20 mg
188 of saponite (SAP) was added to 20 mL of dye solution at the different initial dye
189 concentration at the 100 to 5000 $\text{mg}\cdot\text{L}^{-1}$. The mixture was stirred for 1 h at room
190 temperature and then centrifuged to separate the adsorbent. The concentration of dye in
191 supernatant was analyzed using UV-visible spectrophotometer as described in previous
192 subsection.

193 Experimental results were adjusted to Langmuir [43], Freundlich [44] and
194 Temkin [45] models following the Eqs. (5)–(7):

195

196 Langmuir:
$$\frac{C_e}{q_e} = \frac{1}{K_L q_m} + \frac{C_e}{q_m} \quad (5)$$

197 Freundlich:
$$\ln q_e = \frac{1}{n_F} \ln C_e + \ln K_F \quad (6)$$

198 Temkin:
$$q_e = \frac{1}{n_T} \ln K_T + \frac{1}{n_T} \ln C_e \quad (7)$$

199 Where C_e ($\text{mg}\cdot\text{L}^{-1}$) is the dye equilibrium concentration, q_e ($\text{mg}\cdot\text{g}^{-1}$) is the dye adsorbed
 200 amount on solid/liquid interface, q_{max} ($\text{mg}\cdot\text{g}^{-1}$) is the maximum removal to form a
 201 monolayer of the dye on surface, K_L ($\text{L}\cdot\text{mg}^{-1}$) is the Langmuir constant.

202 In the Freundlich model K_F ($\text{mg}\cdot\text{g}^{-1}$) ($\text{mg}\cdot\text{L}^{-1}$)^{-1/n} and n_F are the Freundlich
 203 constant and a factor which are related to capacity and intensity of the adsorption,
 204 respectively. For Temkin model, n_T is the constant related to adsorption energy
 205 ($\text{J}\cdot\text{mol}^{-1}$), K_T ($\text{L}\cdot\text{mg}^{-1}$) is the Temkin isotherm constant, R is the gas constant (8.314
 206 $\text{J}\cdot\text{mol}^{-1}\cdot\text{K}$) and T is the temperature (K).

207

208 2.6 Synthesis of the hybrid pigments

209

210 1 g of SAP or each O-SAP were dispersed in 100 mL of anthocyanin (RG) citric
 211 acid buffer solution at pH 3 (the RG concentration was $100\text{ mg}\cdot\text{L}^{-1}$) and was left under
 212 stirring for 1 h. The samples were then centrifuged and dried at $50\text{ }^\circ\text{C}$ for overnight. The
 213 hybrid pigments samples are named SAP-RG, β -CD_SAP-RG, CTAB_SAP-RG and β -
 214 CD+CTAB_SAP-RG.

215

216 2.7. Characterizations.

217

218 X-ray diffraction were recorded using D8 Advance Bruker-AXS Powder X-ray
 219 diffractometer with $\text{CuK}\alpha$ radiation ($\lambda = 1.5405\text{ \AA}$). XRD patterns were performed
 220 between $4\text{-}70^\circ$ (2θ) with scan rate of $0.5\text{ deg}\cdot\text{min}^{-1}$.

221 Infrared analyzes were performed on Agilent Cary 630 FTIR spectrometer using
 222 an Agilent diamond Attenuated Total Reflectance (ATR) technique mode, with a

223 spectral resolution $> 2 \text{ cm}^{-1}$ and 32 scans. Spectra were acquired by Microlab FTIR
224 Software (Agilent Technologies) between 4000 and 650 cm^{-1} .

225 Thermogravimetric analyses were carried out using a TA Instrument SDT Q600
226 analyzer. The heating rate was of $5 \text{ }^{\circ}\text{C} \cdot \text{min}^{-1}$ from $25 \text{ }^{\circ}\text{C}$ to $1000 \text{ }^{\circ}\text{C}$, under dry air flow
227 of $10 \text{ mL} \cdot \text{min}^{-1}$, and using alumina pan.

228 TEM study of the samples was performed on a JEOL 2010 microscope, 200 kV
229 LaB₆ coupled Orius camera, from Gatan Company. Samples in the form of bulk
230 powders were suspended in ethanol and then deposited on 400 mesh copper grids
231 covered with an ultrathin carbon membrane of 2–3 nm thickness.

232 MAS NMR spectra were obtained on a Bruker Avance III spectrometer
233 equipped with a 4 mm H-X MAS probe, operating at frequency of 500.17 MHz (¹H),
234 125.77 MHz (¹³C). Chemical shifts were calibrated using the carboxyl signal of
235 adamantane (38.52 ppm) for ¹³C.

236 The ¹³C Cross-Polarization spectra were acquired with a MAS rate of 14 kHz, a
237 ramp-CP contact time of 1 m s and a 1 s recycle delay and with a ¹H decoupling spinal.
238 Over an acquisition time of 40 m s, the number of scans to obtain the spectra depends
239 on the S/N obtained for each sample. Spectra were processed with a zero-filling factor
240 of 2 and with an exponential decay corresponding to a 25 Hz line broadening in the
241 transformed spectra. Only spectra with the same line broadening are directly compared.

242

243

244 **2.8. Chemical and photo-stabilities of the hybrid pigments**

245

246 Chemical stability of anthocyanin molecules loaded on the matrix was verified by
247 exposure of the hybrid pigments to basic and acidic conditions in a desiccator
248 containing aqueous NH₄OH or HCl. At first, the sample was exposed to NH₃
249 atmosphere. After exposure to basic environment, the samples were transferred into a
250 desiccator filled with HCl atmosphere. The sample was exposed to NH₃ and HCl
251 atmospheres, sequentially and repeatedly [23].

252 The photo-stabilities were evaluated by exposure of solid pigments to white light
253 irradiation for 192 h, using a LED lamp set to provide 100 Klx of illumination intensity,
254 in which this time is equivalent to approximately 30 years of exposure in ambient light
255 conditions. To study the effects of irradiation under oxidant and inert atmospheres, the
256 pressed pigments (into pellets) were placed in a desiccator filled with air or nitrogen.

257 The absorbance, reflectance and CIE (Commission Internationale de L'Eclairage)
258 parameters were obtained from an Ocean Optics Halogen and Deuterium Light Source
259 HL-2000-FHSA device as incident light beam and ocean optics USB4000 detector for
260 acquisition. Ocean Optics QP400-1-UV-VIS fiberglass was used to link these devices.
261 For each acquisition, the optimum signal was obtain with an average of 100 scans. The
262 diffuse reflectance (R) converted into equivalent absorption coefficient F(R) using
263 Kubelka–Munk equation (Eq. (1)) [46].

264

$$265 \quad F(R) = \frac{(1-R)^2}{2R} \quad (1)$$

266

267 The “Commission Internationale of l'Eclairage” CIE 1976 color space system was
268 applied to evaluate the color of the pigments. Measurements were done on pressed
269 pellets samples as function of L*, a* and b* coordinates. The differences of colors
270 between unexposed and exposed samples were calculated by
271 $\sqrt{((\Delta L^*)^2 + (\Delta a^*)^2 + (\Delta b^*)^2)}$ equation.

272

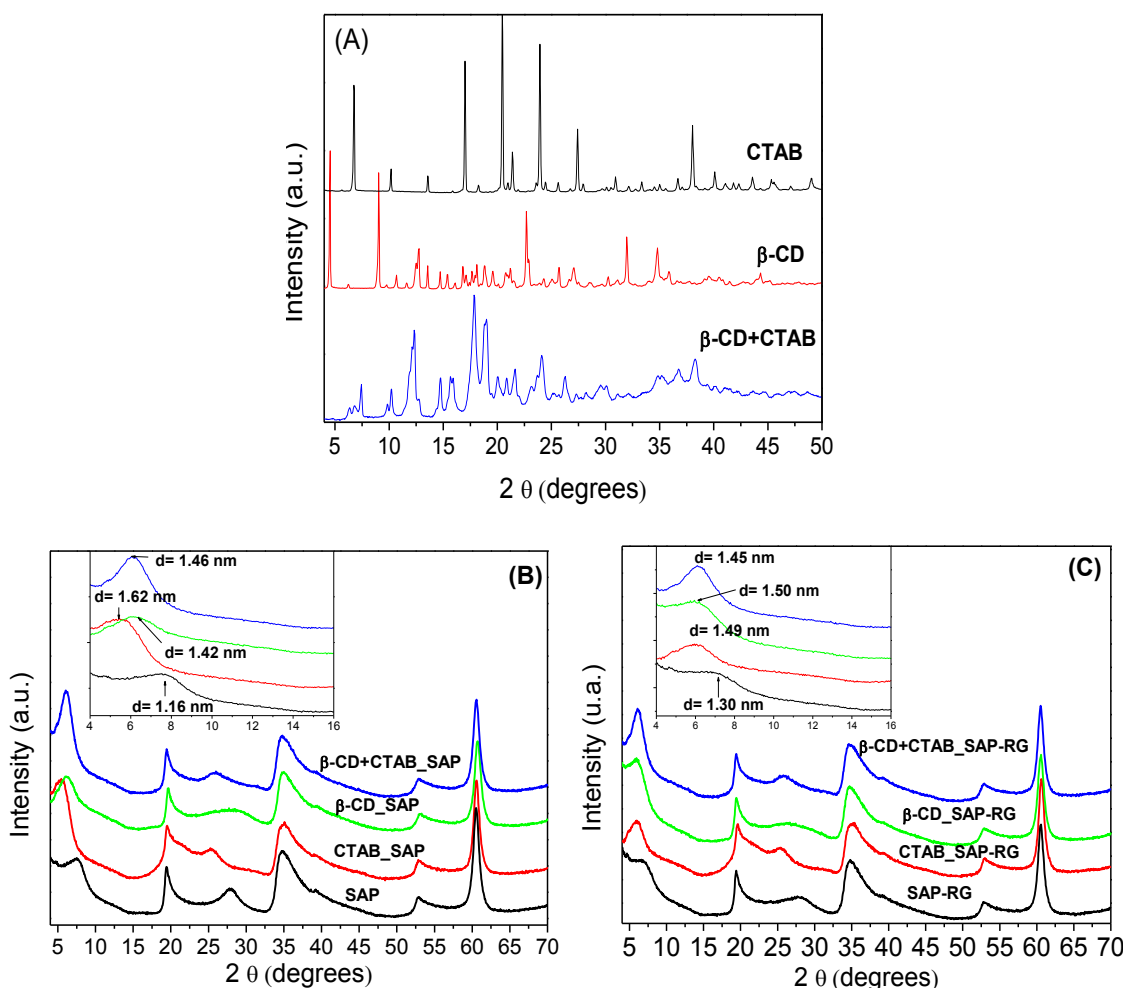
273 **3. Results and Discussion**

274 **3.1 X-Ray Diffraction**

275

276 XRD patterns of the pure CTAB shows typical reflections at 6.83°, 10.23°,
277 13.63°, 16.90°, 20.55°, 21.47°, 23.83°, 37.95°, 40.18 (JCPDS 00-030-1746) (Fig. 1A.).
278 Characteristic reflections of β -CD are observed in 4.53°, 9.04°, 12.70°, 13.58°, 14.75°,
279 17.94°, 18.86°, 21.28°, 22.83°, 24.38°, 25.78°, 27.18°, 32.04° and 34.92° in agreement
280 with previous works [47,48]. The XRD pattern of the product resulting from the mixture
281 of cyclodextrin host and CTAB (β -CD+CTAB inclusion complex) is not a simple
282 mixture of the two precursors but a new crystalline phase [37]. The differences observed
283 between the patterns of their precursors were: i) the absence of the sharp and intense
284 reflections of β -CD and CTAB (i.e. 4.53°, 9.04° for β -CD and 16.90°, for CTAB), ii)
285 other ones shifted (i.e. 14.75°, 18.86° for β -CD and 13.63°, 20.55°, 21.47° for CTAB)
286 and iii) presence of medium intense reflections after complexation (i.e. 14.75°, 18.86°
287 for β -CD and 13.63°, 20.55°, 21.47° for CTAB), due to the encapsulation of the
288 surfactant into the nano-hydrophobic cavities of β -CD [38,39].

289



290

291 **Fig. 1.** X-ray diffractograms of (A) CTAB, β -CD and β -CD+CTAB; (B) SAP,
 292 CTAB_SAP, β -CD_SAP and β -CD+CTAB_SAP; (C) SAP-RG, CTAB_SAP-RG, β -
 293 CD_SAP-RG and β -CD+CTAB_SAP-RG.

294

295 The XRD patterns of the sodium saponite (Fig. 1B) showed typical (hkl)
 296 reflections of the clay and confirmed the success of the synthesis. The reflection at
 297 7.66° (2θ) was associated to the basal spacing, $d_{(001)}$ of 1.16 nm, which can be correlated
 298 with a thickness of monohydrated sodium saponite layer [49].

299 After loading of the organic molecules in SAP, the initial basal spacing increased
 300 to 1.62 nm in CTAB_SAP, 1.42 nm in β -CD_SAP and 1.46 nm in β -CD+CTAB_SAP
 301 (Fig. 1B).

302 Different scenarios can be considered: for CTAB_SAP sample, the process
 303 involves cation exchange between CTA^+ and Na^+ . The orientation of the organic chain
 304 in the interlayer space was suggested considering the dimensions of CTA^+ moieties

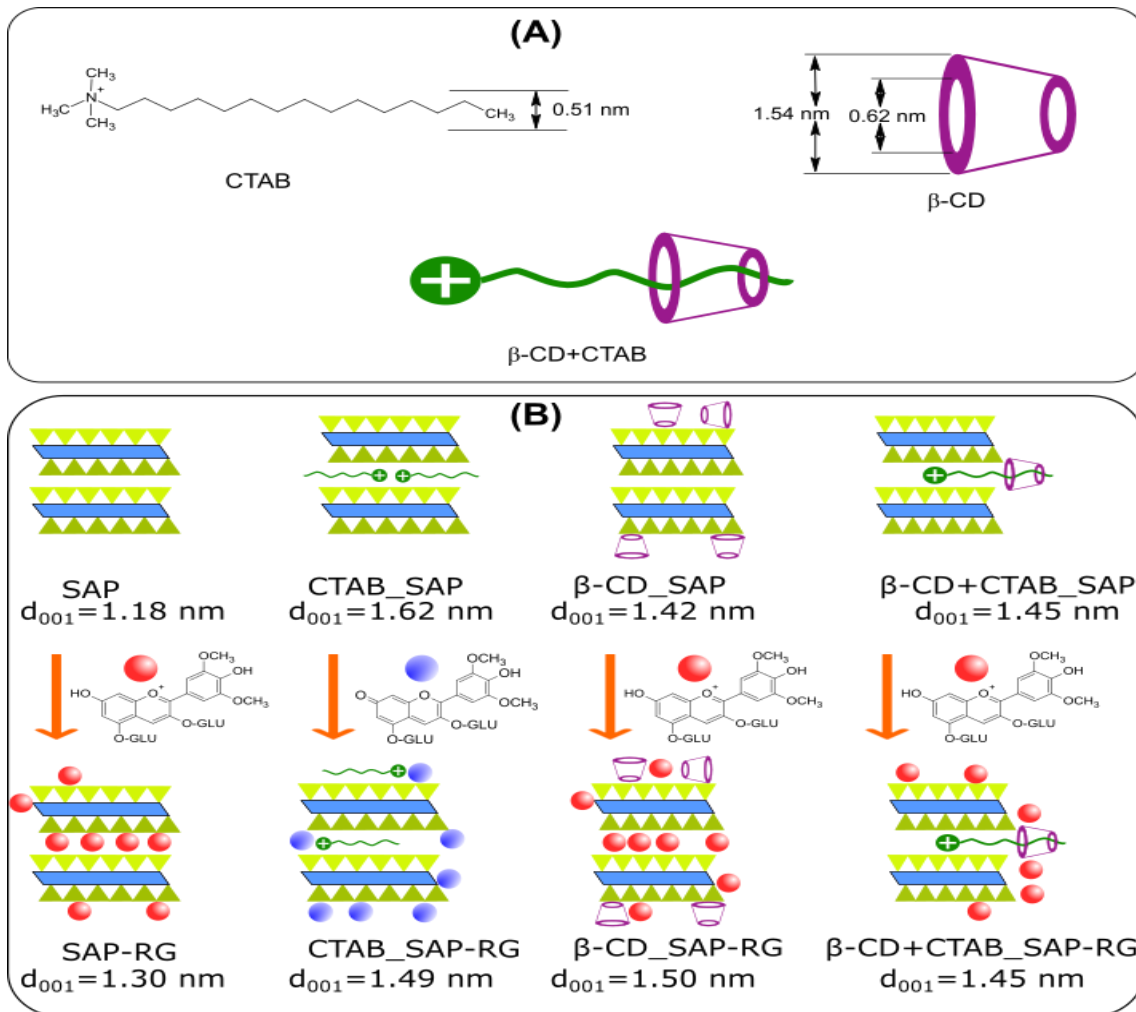
305 (Fig. 2) and the free interlayer space, which value was 0.65 nm for CTAB_SAP,
306 corresponding to the difference between the SAP layer thickness and the basal spacing
307 1.62 nm. Therefore, the results are consistent with a monolayer arrangement of the
308 organic molecules, where the ammonium groups tethered to the clay surface, and the
309 alkyl chains lay parallel to the layers [50].

310 In the β -CD_SAP sample, since the d_{001} didn't increase significantly considering
311 the size of β -CD, one plausible hypothesis is the adsorption of the organic part on the
312 surface of the layers and maybe on the edges via hydrogen bonding.

313 For β -CD+CTAB_SAP, a partial intercalation of the β -CD+CTAB complex can
314 be proposed by ion exchange reaction between interlayer sodium cations of the SAP and
315 positively charged portion of the inclusion complex.

316 For SAP and β -CD-SAP samples loaded with anthocyanin, the (001) reflexion
317 was broader with a slightly increase of $d_{(001)}$ values, suggesting maybe a heterogeneity
318 in the layer stacking due to dye intercalation. For CTAB_SAP after dye loading, the
319 (001) reflexion was also broader but with a slight decrease of $d_{(001)}$ values. In this case, a
320 partial release of of CTA^+ intercalated that convert the anthocyanin from the flavylum
321 cation (AH_2^+) to quinoidal base form (AH) can occur, attenuating the electrostatic
322 repulsions by forming the pair CTA^+/AH on the SAP surface or into interlayer space.
323 This can also explain the blue color of the pigment and the heterogeneity in the layer
324 stacking. However, no change was observed in the d_{001} values of β -CD+CTAB-SAP
325 samples after dye loading suggesting RG loading on the surfaces. Fig. 2 illustrates these
326 all possibilities.

327



329

330

331 **Fig. 2.** Schematic representation of the (A) inclusion complex β -CD+CTAB and (B)
332 hybrid formation.

333

334 3.2 Morphological analysis

335

336 TEM micrographs showed layers with alternate dark and bright fringes allowing
337 the measurement of interplanar distances.

338 For pristine SAP, an interlayer distance of 1.19 ± 0.11 nm was obtained (Fig. 3A).

339 In O-SAP samples, the interlayer distance increased to 1.57 ± 0.19 nm, 1.41 ± 0.13 nm and

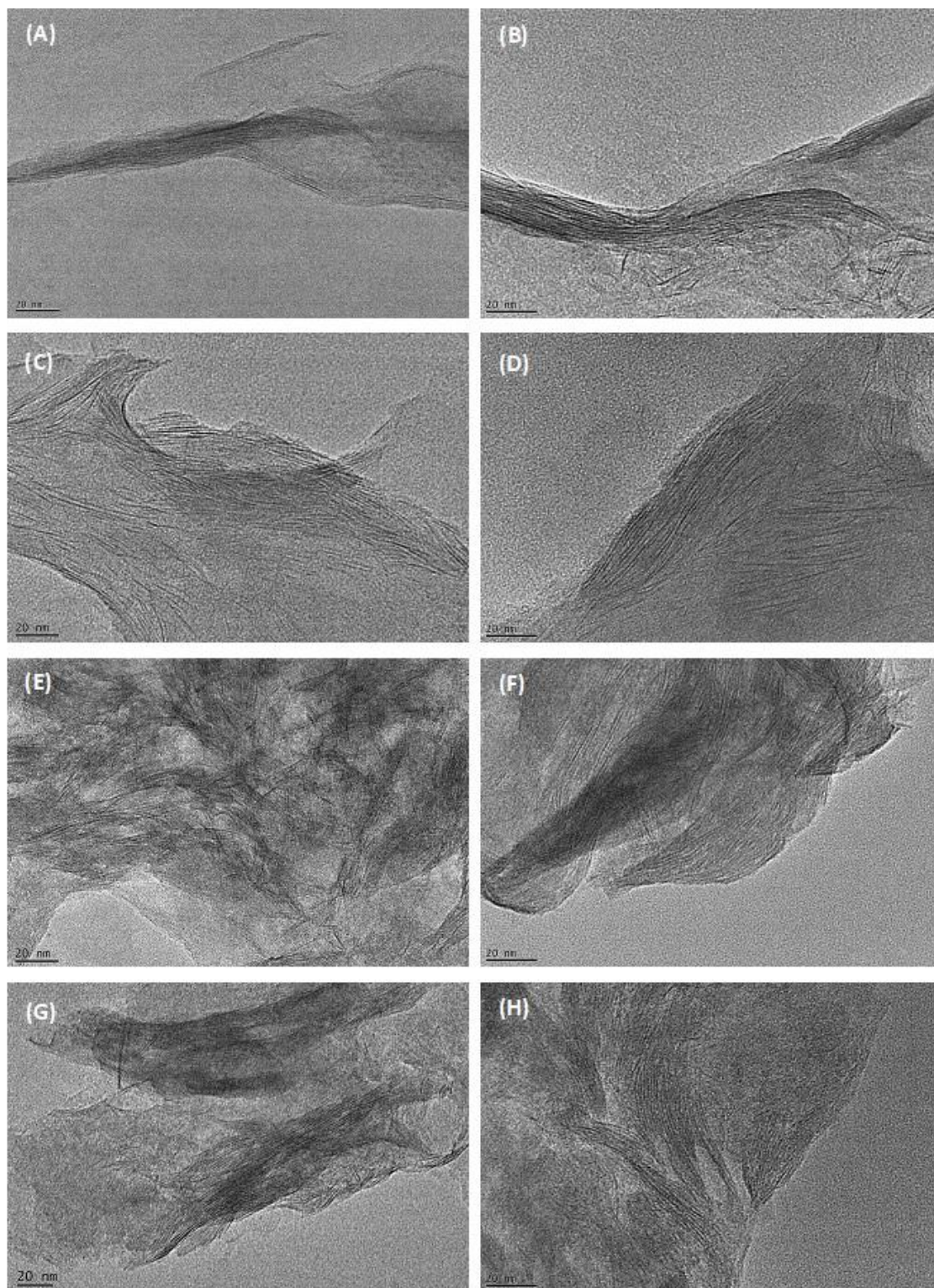
340 1.43 ± 0.13 nm for CTAB_SAP, β -CD_SAP and β -CD+CTAB_SAP respectively (Fig. 3

341 C;E and G). After loading the anthocyanin molecules, the d_{001} spacing were 1.39 ± 0.19 ,

342 1.49 ± 0.20 , 1.51 ± 0.19 and 1.43 ± 0.19 nm for SAP-RG, CTAB_SAP-RG, β -CD_SAP-RG

343 and β -CD+CTAB_SAP-RG, respectively (Fig. 3 B;D;F and G). The values corroborated

344 with the XRD data.



345

346 **Fig. 3.** TEM images of (A) SAP; (B) SAP-RG; (C) CTAB_B_SAP; (D) CTAB_B_SAP-RG;
 347 (E) β -CD_SAP; (F) β -CD_SAP-RG; (G) β -CD+CTAB_B_SAP and (H) β -
 348 CD+CTAB_B_SAP-RG.

349

350 3.3 FTIR

351

352 The infrared spectra of pure β -CD indicated its main absorptions at 3280 and 2925
353 cm^{-1} (Fig. 4A) attributed to $\nu(\text{O-H})$ and $\nu(\text{C-H})$, as well as the bands at 1152, 1077,
354 1023, and 940 cm^{-1} (Fig. 4B) assigned to $\delta(\text{O-H})$, $\nu(\text{C-C})$, and the α -1,4 linkage
355 skeletal vibration, respectively [51,52].

356 The main bands associated to CTAB occurred at 3016, 2916 and 2847 cm^{-1} and
357 were attributed to the $\text{N}(\text{CH}_3)_3$ asymmetric vibration, C-H and CH_2 asymmetric and
358 symmetric stretching, respectively. Other bands in the range 1460-1488 cm^{-1} were
359 assigned to $[\text{N}(\text{CH}_3)_3]$ and (CH_2) bending modes, while C-N vibrations were detected at
360 911 cm^{-1} and 963 [53,54].

361 The formation of the $(\beta\text{-CD})\text{-}(\text{CTAB})$ complex attenuated the surfactant
362 absorptions, due to the seven repeating units in the β -CD, the spectrum of the inclusion
363 complex was largely dominated by the bands of the host portion, but even so, the
364 spectra in Fig. 4A and Fig. 4B display some differences in comparison to spectra of
365 their precursors that suggest the inclusion of CTAB into the β -CD cavity [51]. The band
366 at 3280 cm^{-1} assigned to O-H stretching may correspond to the new hydrogen bonds in
367 the complexes. The region between 2800-2980 cm^{-1} is attributed to $\nu(\text{C-H})$ in β -
368 $\text{CD}+\text{CTAB}$: it shows the contributions of the (CH) group in β -CD, shifted from 2925
369 cm^{-1} to 2919 cm^{-1} , and also a weak band at 2852 cm^{-1} related to the contribution of
370 (CH_2) stretching of CTAB, which appears as a shoulder probably due to the attenuation
371 providing by the inclusion in the β -CD cavity. The bands at 1460-1488 cm^{-1}
372 disappeared also suggesting the inclusion of the aliphatic chains in β -CD cavity, since
373 these bands are mostly associated to the (CH_2) bending [55].

374 In Fig. 4C are shown the spectra of pristine SAP and the organoclays formed by
375 intercalation of the surfactant, cyclodextrin and the inclusion complex represented by
376 the CTAB_SAP, β -CD_SAP, β -CD+CTAB_SAP respectively.

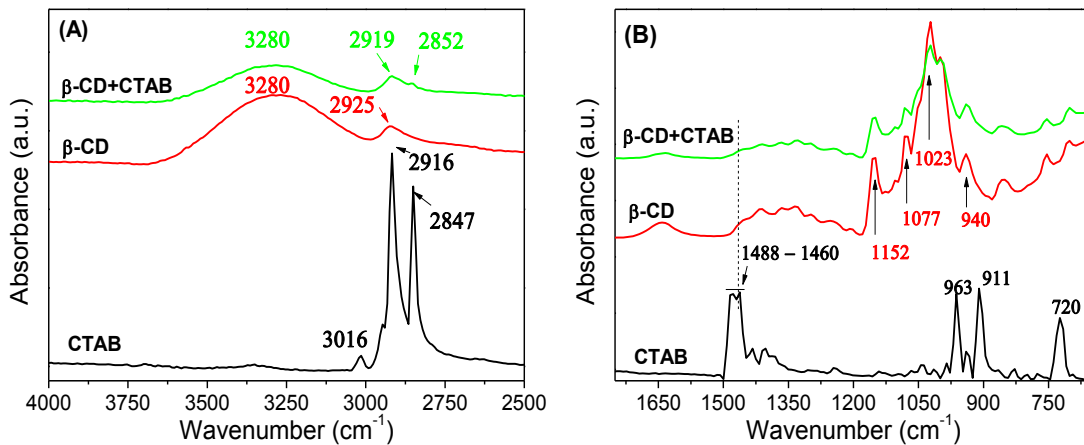
377 For the SAP sample, the sharp and weak band at 3677 cm^{-1} and the region
378 between 3000-3600 cm^{-1} are assigned to $-\text{OH}$ vibrations modes. The band at 1633 cm^{-1}
379 is attributed to $-\text{OH}$ water bending. The band at 980 cm^{-1} was assigned to the Si-O-Si
380 stretching [4,56].

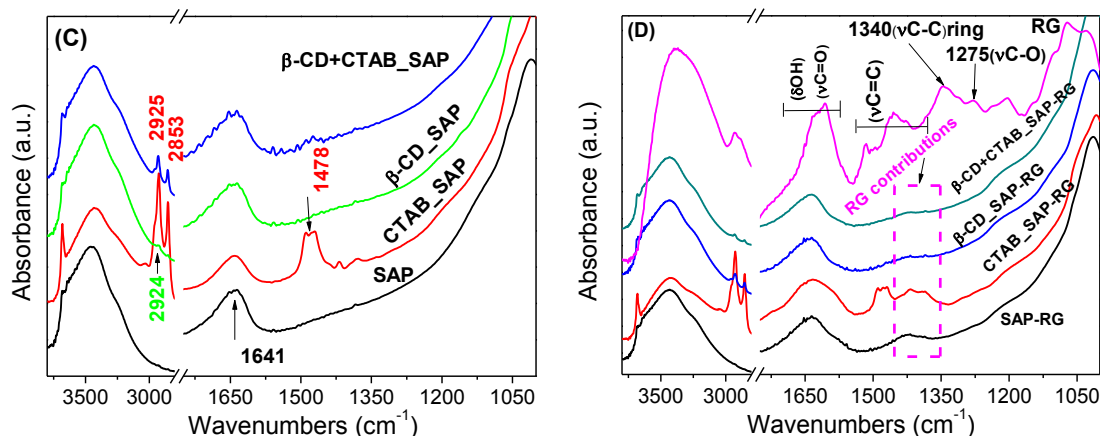
381 After organomodification (Fig. 4C), the changes in CTAB_SAP spectra that
382 confirm the presence of organic molecules are the new bands at 1478, 2847 and 2925,

383 cm^{-1} , which were assign to the characteristic vibrations of CTAB alkyl chain.
 384 Concerning the β -CD_SAP spectrum, the different shape of the OH stretching and
 385 bending modes compared to the ones present in the pristine SAP suggests the
 386 contributions of OH groups brought from polysaccharide. A weak band at about 2924
 387 cm^{-1} is attributed to $\nu(\text{CH})$. Finally, the β -CD+CTAB_SAP sample shows more intense
 388 bands at 2853 and 2925 attributed to the CTAB alkyl chain in the β -CD+CTAB
 389 inclusion complex, in addition to the similar characteristics observed for β -CD_SAP.

390 The Fig. 4D presents the spectra of the natural dye (RG) and the hybrid pigments
 391 obtained. In the RG spectrum, the main bands related to the aromatic and phenolic
 392 structure of the anthocyanin can be seen in the following regions : 1250-1370 cm^{-1} and
 393 1350-1530 cm^{-1} attributed to C-O and C-C modes, respectively [17,18], 1550-1700
 394 cm^{-1} assigned to O-H bending and C=O stretching; and 3000-3700 cm^{-1} associated with
 395 stretching vibrations of O-H.

396 The presence of anthocyanin in the hybrids can be verified by the distinguished
 397 signal of -OH stretching and bending modes due to the contributions of anthocyanin
 398 bands and the appearance of the corresponding peaks in the region of 1320-1450 cm^{-1} ,
 399 emerging in the FTIR spectrum of the hybrids.





400

401 **Fig. 4.** FTIR spectra of (A-B) CTAB, β -CD and the inclusion complex β -CD+CTAB;
 402 (C) SAP and the organo-clay formed after incorporate CTAB, β -CD and β -CD+CTAB
 403 molecules; (D) hybrid pigments formed after adsorption of anthocyanin dye molecule in
 404 SAP, CTAB_SAP, β -CD_SAP and β -CD+CTAB_SAP.

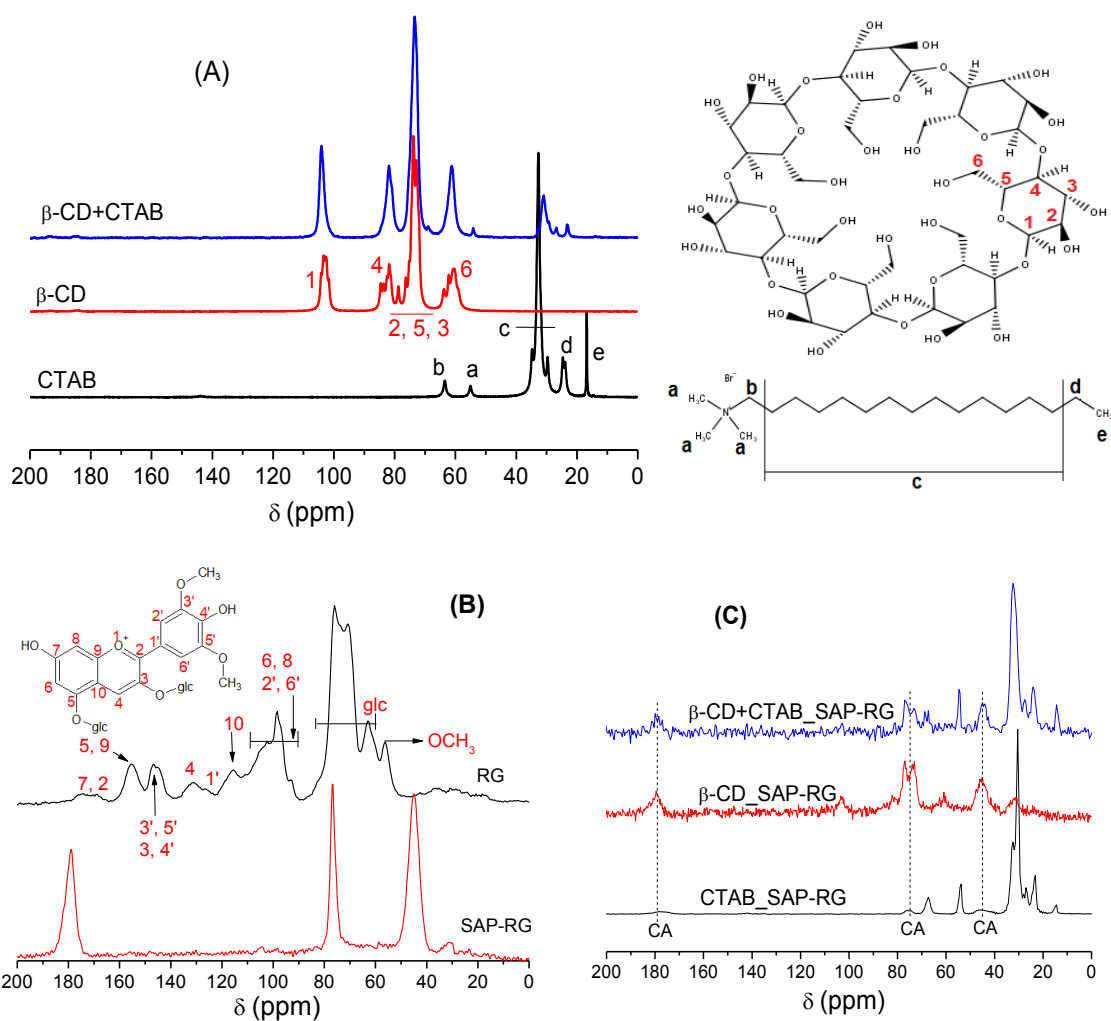
405

406 3.4 ^{13}C MAS NMR

407

408 ^{13}C MAS NMR spectra of β -CD+CTAB and their precursors are presented in Fig.
 409 5A. The signals of CTAB occur in the chemical shift range of 10–70 ppm. The
 410 resonances at 16 ppm, 24 ppm and the complex signals that appear at 27–38 ppm are
 411 assigned to the terminal methyl group, the final methylene near to terminal methyl and
 412 the internal methylenes of the alkyl chain, respectively. The resonances at 55 ppm and
 413 63 ppm are related to the N-CH₃ of the head-group and the first methylene group
 414 directly bonded to nitrogen, respectively [57]. The spectrum of β -CD shows the
 415 resonances of C1, C4 and C6 as multiple peaks that are spread over the chemical shift
 416 range of 100–107 ppm, 80–86 ppm and 57–65 ppm, respectively. It occurs due to
 417 asymmetric glucopyranosyl conformations. The chemical shift range of 68–77 ppm is
 418 related to the signals of C2, C5 and C3 [58].

419



420

421 **Fig. 5.** ^{13}C MAS NMR spectra of (A) $\beta\text{-CD}+\text{CTAB}$ and their precursors, (B) RG and
 422 SAP-RG, (C) CTAB_SAP-RG, $\beta\text{-CD}_\text{SAP-RG}$ and $\beta\text{-CD}+\text{CTAB}_\text{SAP-RG}$.

423

424 The spectra of $\beta\text{-CD}+\text{CTAB}$ complex (Fig. 5A) shows differences in comparison
 425 with the precursors. The resonances related to $\beta\text{-CD}$ carbons appeared without
 426 significant shifts but as sharp singlet peaks after complexation, which implies that the $\beta\text{-}$
 427 CD unit adopts a symmetric cyclic conformation with the inclusion of CTAB alkyl
 428 chain. Changes in chemical shift confirm the interaction, as occurred in C(4) and C(6)
 429 glucopyranosyl monomer signals. For the CTAB signals, the peak assigned to terminal
 430 methyl group is absent, the peaks of methylene shifted from 24 ppm to 23 ppm and the
 431 complex signals related to internal methylenes shifted from the region of 27-38 ppm to
 432 25-34 ppm. These changes indicate the inclusion of alkyl chain into $\beta\text{-CD}$ hydrophobic
 433 cavity [39].

434 The ^{13}C MAS NMR spectra of the RG and the RG-SAP are presented in Fig. 5B,
435 C. In the RG spectrum: the signal at 56 ppm is attributed to the OCH_3 groups bounded
436 to the aglycone portion in $\text{C}(3')$ and $\text{C}(5')$ and the signals between 58-85 ppm are
437 assigned to the chemical shifts of the glycosidic portions. The signals above 90 ppm are
438 attributed to the aromatic carbons in flavylum cation, as indicated in Fig. 5B [59,60].

439 After incorporation of RG in SAP, any peaks in ^{13}C MAS NMR spectrum of the
440 dye molecule was observed in the hybrid probably dominated by the other
441 contributions. On the other hand, three signals at 45 ppm, 76 ppm and 179 ppm were
442 assigned to the citric acid, which was also incorporated during the adsorption process.
443 The same behavior is observed for CTAB_SAP-RG, β -CD_SAP-RG and β -
444 CD+CTAB_SAP-RG (Fig. 5C) hybrids that showed peaks assigned to the organic
445 precursors and also three signals of the citric acid (CA).

446

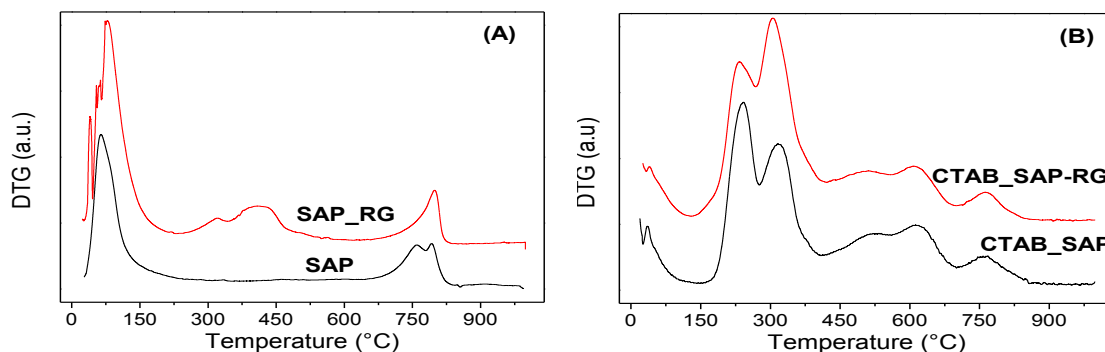
447 3.5 Thermal analyses

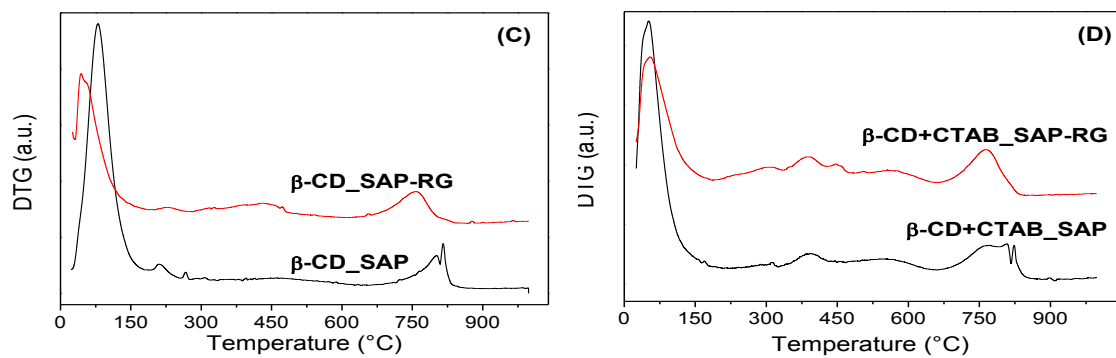
448

449 In Fig. 6A, the first step of degradation at 25-238 $^\circ\text{C}$ (mass loss about 8%) for raw
450 SAP was assigned to the loss of physisorbed water and dehydration of interlayer
451 cations. The second event at 640-859 $^\circ\text{C}$ is due to dehydroxylation of SAP with a
452 weight loss of 3% [24,27]. DTG of SAP-RG shows an additional weight loss of 7% in
453 the region 210-623 $^\circ\text{C}$ assigned to the degradation of the incorporated anthocyanin.

454 The weight losses in the second thermal event of O-SAP samples before the RG
455 adsorption (Fig. 6B-D, Table 1) were 2%, 6% and 30% in β -CD_SAP, β -
456 CD+CTAB_SAP and CTAB_SAP respectively. After dye loading, the organic mass
457 losses increases to 6%, 8% and 32% for β -CD_SAP-RG, β -CD+CTAB_SAP-RG and
458 CTAB_SAP-RG, respectively.

459





460

461 **Fig. 6.** DTG curve of (A) SAP and SAP-RG; (B) CTAB_SAP and CTAB_SAP-RG; (C)
 462 β -CD_SAP and β -CD_SAP-RG; (D) β -CD+CTAB_SAP and β -CD+CTAB_SAP-RG.

463

464

465 **Table 1.** Temperature range and percentages of mass loss observed in DTG curves.

Sample	Temperature (°C)	Mass loss (%)
SAP	25-238	8.0
	640-859	3.5
SAP-RG	25-210	13.0
	210-623	7.2
	623-878	3.6
CTAB_SAP	25-117	2.4
	117-710	29.5
	710-878	2.9
CTAB_SAP-RG	25-125	2.4
	125-702	32.2
	702-888	2.5
β -CD_SAP	25-174	15.6
	174-319	2.5
	685-864	2.9
β -CD_SAP-RG	25-182	9.3
	182-600	5.9
	600-885	3.6
β -CD+CTAB_SAP	25-180	9.6
	180-670	6.1
	670-892	3.1
β -CD+CTAB_SAP-RG	25-181	6.5
	181-667	7.9
	667-885	3.0

466

467 3.6 Adsorption studies

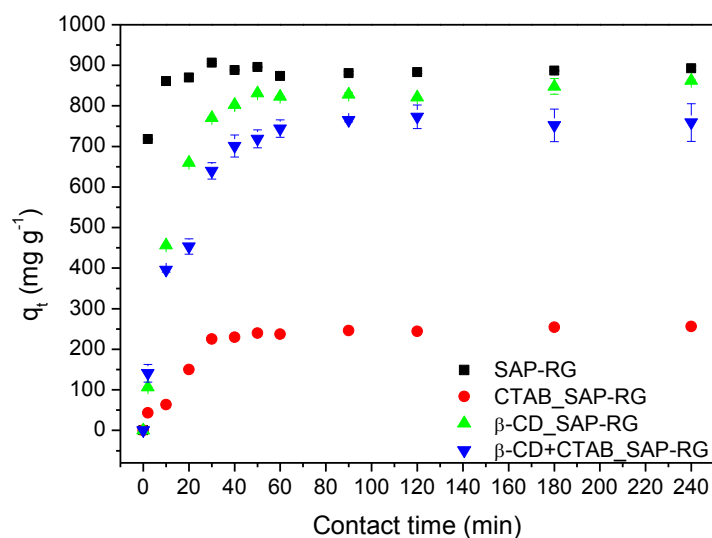
468

469 3.6.1 Effect of the contact time

470

471 Adsorption kinetics studies were carried out and are depicted in Fig. 7.

472



473

474 **Fig. 7.** Influence of the contact time on the RG adsorption on SAP; CTAB_SAP; β-
 475 CD_SAP; β-CD+CTAB_SAP samples.

476

477 The adsorption was fast during the first few minutes, mainly for raw saponite. The
 478 equilibrium times were reached after 10 min and resulted in dye adsorption capacity
 479 close to 910 mg·g⁻¹ for SAP. For organo-saponite samples, the equilibrium times were
 480 achieved after 30, 50 and 60 min for CTAB_SAP, β-CD_SAP and β-CD+CTAB_SAP
 481 respectively, with lower maximum dye adsorption capacity than the pristine saponite. It
 482 is an indicative of the presence of different adsorption sites on organo-saponites.

483 In order to better understand the adsorption kinetics, the pseudo-first-order,
 484 pseudo-second-order and Elovich models were applied to experimental data and the
 485 resulted kinetic parameters of the fittings are presented in Table 2.

486 All systems were well-fitted to the pseudo-second order model, since that higher
 487 R² coefficient and low difference between the q_{e,exp} and q_{e,theor} were observed. Same
 488 results were obtained in other works [27,61].

489

490

491 **Table 2.** Kinetic parameters obtained by fitting the experimental data to pseudo-first
 492 order, pseudo-second order and Elovich models in the RG adsorption data by the
 493 organo-saponites.

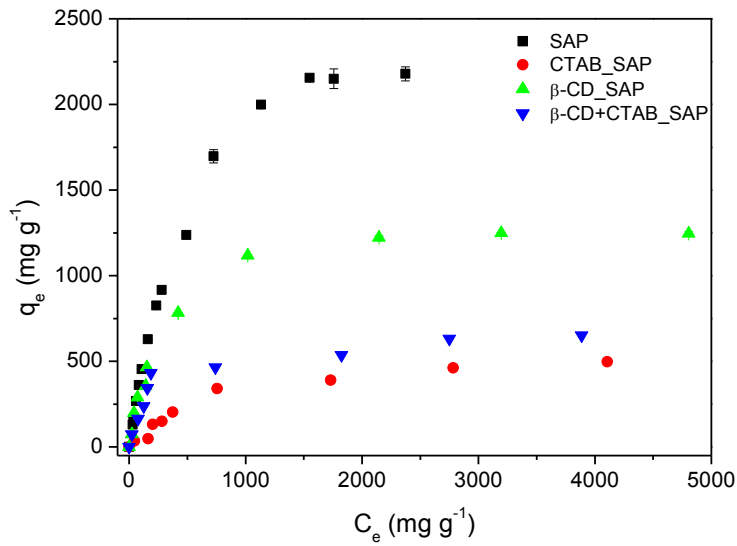
Pseudo-first order				
Hybrid	$q_{e,exp}$ ($mg \cdot g^{-1}$)	$q_{e,cal}$ ($mg \cdot g^{-1}$)	k_1 $10^{-2} (min^{-1})$	R^2
SAP	906.71	45.30	0.57	0.2278
CTAB_SAP	256.02	118.21	2.43	0.8289
β -CD_SAP	862.09	234.27	1.83	0.6138
β -CD+CTAB_SAP	773.30	111.94	2.74	0.0411
Pseudo-second order				
Hybrid	$q_{e,exp}$ ($mg \cdot g^{-1}$)	$q_{e,cal}$ ($mg \cdot g^{-1}$)	K_2 10^{-2} ($g \cdot mg^{-1} \cdot min^{-1}$)	R^2
SAP	906.71	892.86	243.89	0.9999
CTAB_SAP	256.02	273.22	7.59	0.9891
β -CD_SAP	862.09	892.86	13.49	0.9979
β -CD+CTAB_SAP	773.30	793.65	13.32	0.9976
Elovich				
Hybrid	$q_{e,exp}$ ($mg \cdot g^{-1}$)	α ($mg \cdot g^{-1} \cdot min^{-1}$)	β $10^{-2} (g \cdot mg^{-1})$	R^2
SAP	906.71	$6.02 \cdot 10^{12}$	3.43	0.5653
CTAB_SAP	256.02	58.58	1.94	0.8179
β -CD_SAP	862.09	360.84	0.64	0.8313
β -CD+CTAB_SAP	773.30	284.55	0.72	0.8732

494

495 3.6.2 Effect of the initial dye concentration

496

497 Equilibrium isotherms are presented in Fig. 8. The equilibrium curves showed
 498 first an increasing in the adsorption capacity at high RG concentrations. Then a plateau
 499 is observed corresponding to the saturation of the active sites [62–64].



500

501 **Fig. 8.** Influence of the RG initial concentration on the adsorption process of SAP;
 502 CTAB_SAP; β -CD_SAP; β -CD+CTAB_SAP.

503

504 The saturation occurred at high RG initial concentration and resulted in high
 505 adsorption capacity for SAP-RG, (3500 mg·L⁻¹ RG initial concentration and adsorption
 506 capacity about 2170.0 mg·g⁻¹). However for organo-saponite samples, equilibrium
 507 occurred at 3000.0, 1000.0 and 2500 mg·L⁻¹ of RG initial concentrations and showed
 508 adsorption capacities close to 1230.0, 640 and 470 mg·g⁻¹ for β -CD_SAP, β -
 509 CD+CTAB_SAP and CTAB_SAP respectively.

510 The equilibrium data were adjusted to Langmuir, Freundlich and Temkin models,
 511 and the resulting parameters are summarized in Table 3. The values of isotherm
 512 correlation coefficients revealed that the experimental data were well-fitted to Langmuir
 513 (R^2 closer to 1) compared with other models. Additionally, the R_L values calculated
 514 from the Langmuir equation suggested that the adsorption was favorable ($0 < R_L < 1$) in
 515 all cases. Adsorption sites in each sample were uniformly distributed on the surface and
 516 a monolayer adsorption took place [65].

517

518

519

520

521

522 **Table 3.** Parameters obtained by fitting the experimental data to Langmuir, Freundlich
 523 and Temkin models in the RG adsorption by the organo-saponites.

Langmuir				
Hybrid	$q_{e,exp}$ (mg·g ⁻¹)	q_{max} (mg·g ⁻¹)	R_L	R^2
SAP	2178.48	2819.06	0.21	0.9924
CTAB _B _SAP	462.24	595.24	0.66	0.9615
β-CD_SAP	1222.97	1343.35	0.19	0.9978
β-CD+CTAB _B _SAP	632.14	671.14	0.26	0.9967
Freundlich				
Hybrid	n_F (mg·g ⁻¹)	K_F (mg·g ⁻¹)(mg·L ⁻¹) ^{-1/n}		R^2
SAP	1.52	18.84		0.9596
CTAB _B _SAP	1.73	4.73		0.8716
β-CD_SAP	2.10	31.83		0.8797
β-CD+CTA_SAP	2.92	42.74		0.8025
Temkin				
Hybrid	n_T (J·mol ⁻¹)	K_T 10 ⁻² (L·mg ⁻¹)		R^2
SAP	4.63	2.72		0.9646
CTAB _B _SAP	21.75	1.74		0.9512
β-CD_SAP	10.00	4.98		0.9675
β-CD+CTAB _B _SAP	23.20	10.63		0.9322

524

525 3.7 Chemical and photo-stabilities of the hybrid pigments

526 3.7.1 Spectra changes

527

528 The UV-Vis spectra of RG in citric acid solution buffered at pH 3 showed an
 529 absorption at 525 nm (Fig. 9A). The majority of anthocyanin molecules present in RG
 530 are malvidin-3,5-diglucoside, therefore the results are in concordance with the literature,
 531 that shows absorption around 520 nm for acid solution of anthocyanin [11,12,66].

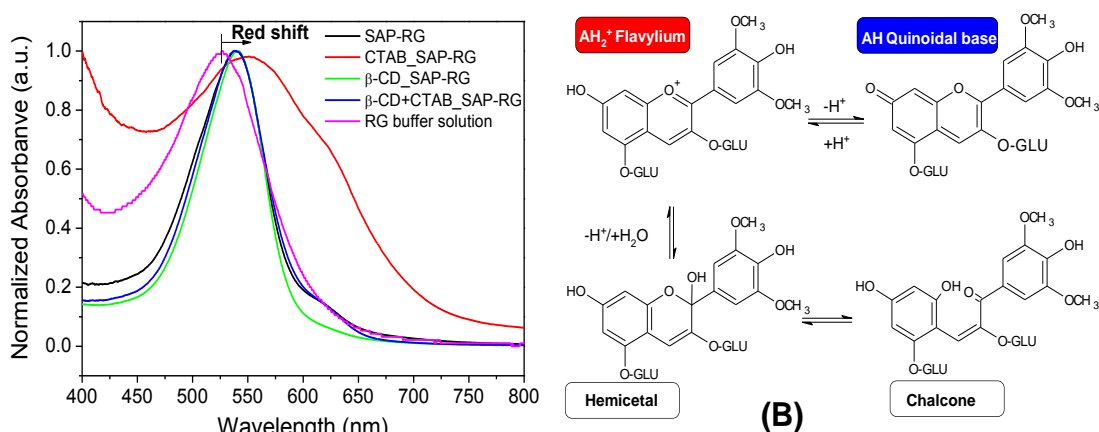
532 The Fig. 9B shows the possible structural transformations of anthocyanin
 533 molecules in aqueous solution. The flavylium is the most stable form of anthocyanin
 534 that appears redish and turns to blue after conversion to quinoidal base when pH
 535 increases and finally to non- colored chalcone via hemiacetal form.

536 Comparing the spectra of RG solution with those of hybrid pigments, a red shift
 537 occurred from 525 to 539 nm for SAP-RG, β-CD_SAP-RG, β-CD+CTAB_B_SAP-RG
 538 samples and 554 nm for CTAB_B_SAP-RG. The pH was adjusted by the addition of citric
 539 acid buffer solution during the hybrid pigment formation. Shifts in the absorptions can

540 be related to electrostatic interactions between the clay mineral layer and the dye and/or
 541 by intramolecular interaction between the organic moieties in the respective hybrids.

542 The shift and presence of a broad band in the spectrum of CTAB_SAP-RG may
 543 indicate the deprotonation of the flavylium cations into deprotonate quinoidal base AH_2
 544 \rightleftharpoons AH, which can be stabilized by electrostatic interaction with the positively
 545 charged surfactant in this hybrid system. This behavior may explain the blue color of
 546 the hybrid, while the other ones were weakly red.

547



548 **Fig. 9.** (A) Diffuse reflectance UV-Vis spectra of hybrid pigments and the spectrum of
 549 RG citric acid buffer solution pH 3; (B) schematic representation of possible
 550 anthocyanin structures in different pHs in aqueous solution.

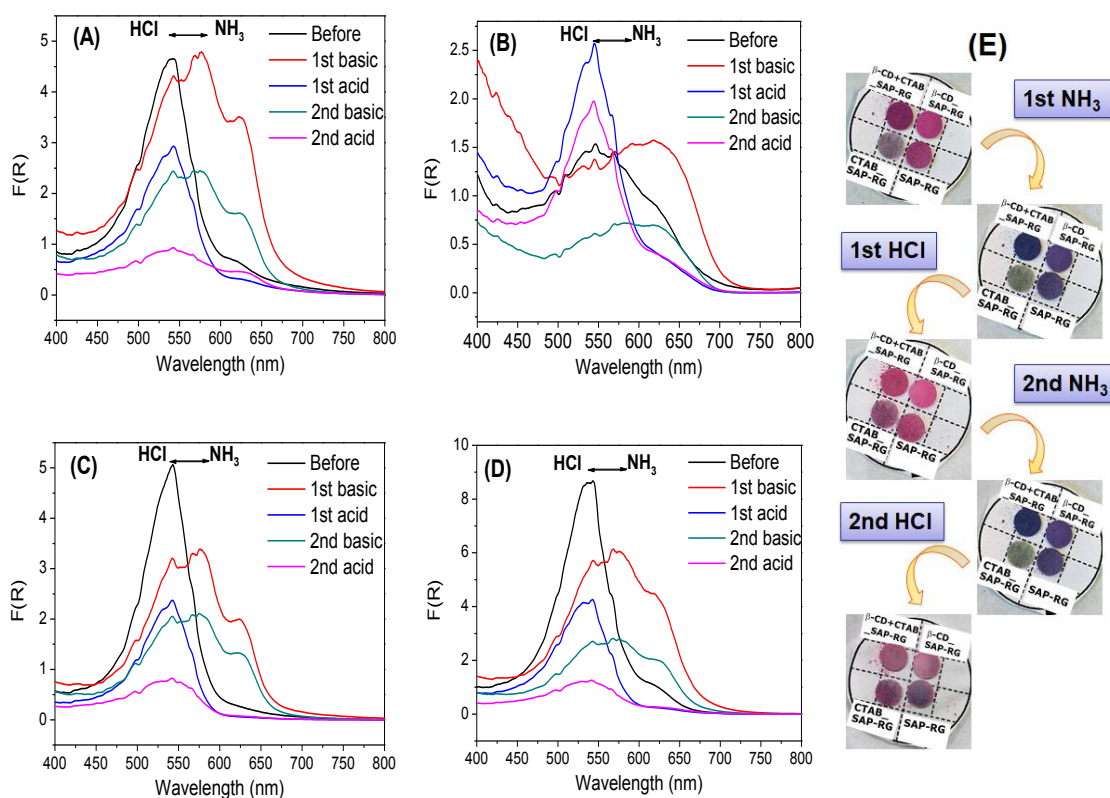
551

552 3.7.2 Color changes in acid/basic environments

553

554 The hybrid pigments were exposed to acidic or basic atmosphere prepared in a
 555 desiccator, in which the samples were submitted to HCl or NH₄OH atmosphere. The
 556 results upon exposure to acidic and basic vapors were monitored by visible absorption
 557 spectroscopy and also by visual changes in their photographs, these results are present
 558 in Fig. 10.

559



560 **Fig. 10.** Spectra changes after exposure to acidic and basic environments for (A) SAP-
 561 RG; (B) CTAB_SAP-RG; (C) β -CD_SAP-RG and (D) β -CD+CTAB_SAP-RG. (E)
 562 Digital photographs of the color changes of hybrid pigments upon exposure.

563

564 Colors changes from red to blue after exposure to basic atmosphere (NH_3 from
 565 aqueous NH_4OH) were observed in the SAP-RG, β -CD_SAP-RG and β -
 566 CD+CTAB_SAP-RG. The process is reversible, as shown in Fig. 10E. The exposure
 567 time to change the color was about 10 min. Similar results were obtained in the
 568 literature.

569 In Fig. 10(A, C and D), the absorption band have a redshift after exposure to basic
 570 atmosphere, and return to the same wavenumber, after exposure to basic atmosphere.
 571 After several cycles; the same observations on the spectra were noticed. The color
 572 change was reversible and repeatable for at least two cycles. The color changes are still
 573 observed after the second cycle of exposure, although strong acid and base conditions
 574 degraded the pigments.

575 The contribution of quinoidal base in the anthocyanin molecule in CTAB_SAP-
 576 RG was more pronounced than in the other hybrids and explains its initial blue color.
 577 After the first exposure to basic vapor, the right shift observed in Fig. 10B is due to the

578 conversion of remaining flavylium cations to quinoidal base, which causes a change
579 only in nuance of blue (Fig. 10E). Hybrids being exposed to basic conditions were again
580 submitted to acidic environment, the color change to red and their spectra were similar
581 to the other hybrids and indicated that the anthocyanin molecules became in flavylium
582 cation form. The behavior of color change in the following cycles was also similar to
583 the others hybrid pigments [18,20,23,32].

584 The decrease in relative absorbance is 80.4%, 73.8%, 83.2% and 84.3% for SAP-
585 RG, CTAB_SAP-RG, β -CD_SAP-RG and β -CD+CTAB_SAP-RG respectively. These
586 data indicate that the CTAB_SAP-RG has a slightly better chemical stability than the
587 other pigments, since it has lowest decrease of relative absorbance after four cycles of
588 acid basic exposure.

589

590 3.7.3 Photostability

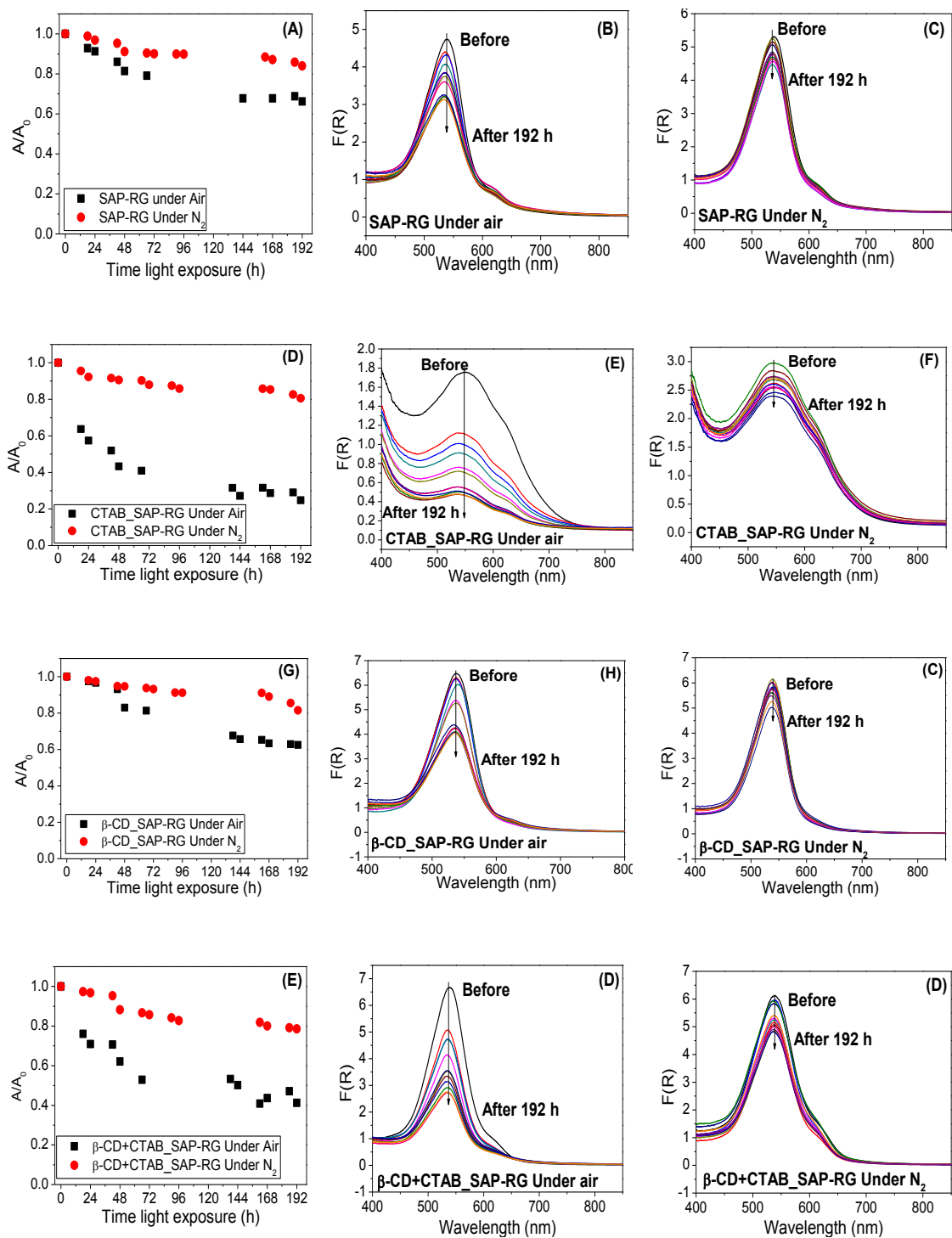
591

592 The photostability of the hybrid pigments were studied under LED light exposure
593 for 192 h under air and nitrogen atmosphere. Fig. 11 depicts the UV-Vis spectra.

594 The progressive decreasing in the absorbance at maximum wavelength occurred
595 without differences in the spectral patterns, which indicated no simultaneous reaction
596 that could form different derivatives chromophore species during the light exposure.
597 Degradation were most pronounced in the process carried out under air for all hybrids.
598 This behavior is expected since the photodegradation is often considered in relation to
599 the oxidation caused by the evolution of singlet oxygen $^1\text{O}_2$ [12]. The order of fading of
600 the hybrid pigments under air followed, CTAB_SAP-RG (75%) > β -CD+CTAB_SAP-
601 RG (59%) > β -CD_SAP-RG (37%) > SAP-RG (34%).

602 On the other hand, the degree of degradation were about 18% (based on $A/A_0 =$
603 0.82) for all hybrids under nitrogen atmosphere. The time exposure of the samples
604 confirmed that the RG degradation process was less pronounced. Under nitrogen,
605 reactive species are more difficult to form but the oxidation process remains possible
606 due to the residual water molecules present in the pigments.

607

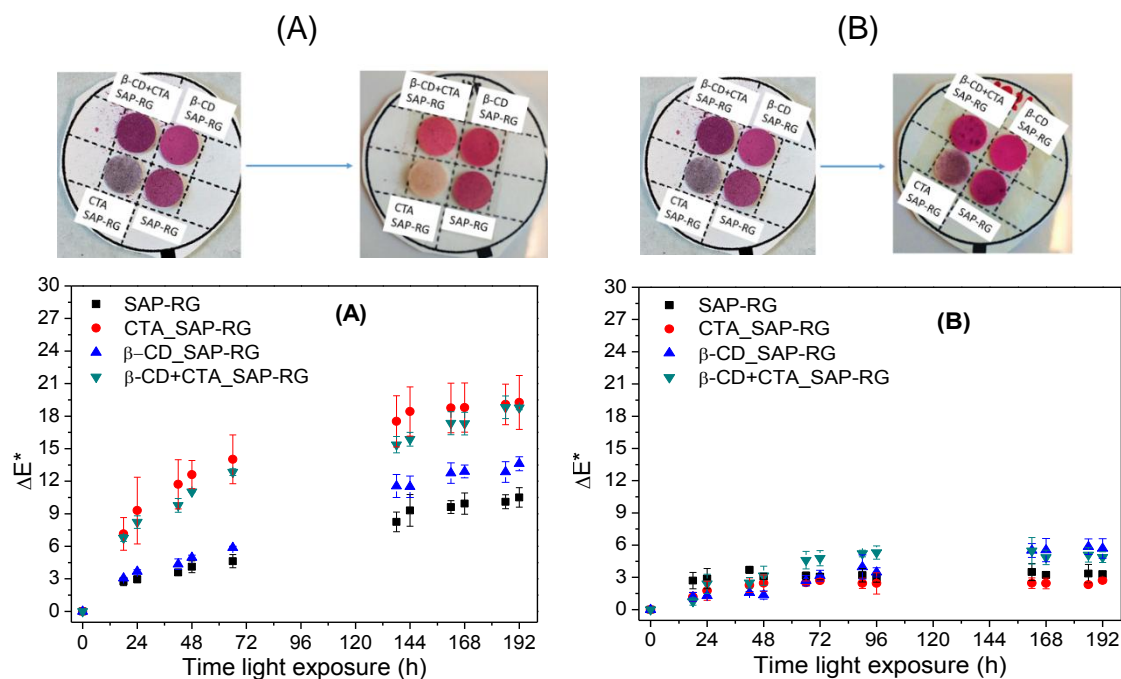


608

609 **Fig. 11.** Relative absorbance at λ_{max} and evolution of spectral patterns during light
 610 exposure for 192 h under air and nitrogen atmosphere for (A), (B) and (C) SAP-RG;
 611 (D), (E) and (F) CTAB_SAP-RG; (G), (H) and (I) β -CD_SAP-RG; (J), (K) and (L) β -
 612 CD+CTAB_SAP-RG.

613 The colors of solid hybrid pigments were evaluated before and after light exposure
614 during 192 h (30 years of exposure in a museum). Measurements of L*a*b* parameters
615 were carried out at different light irradiation times (Fig. 12).

616



618

619 **Fig. 12.** Photo-ageing of pigments followed by color change observations over
 620 192 h of light exposure under (A) air and (B) nitrogen atmosphere.

621

622 In solution, the color of RG changes from red in acid conditions to blue in neutral
 623 to weak alkaline conditions. However, the difference in color presented by the hybrids
 624 results from the different interactions between the host and the guest since the effect of
 625 pH on the color was controlled with the citric acid buffer solution. The color for SAP-
 626 RG is probably due to the intercalation of RG molecule in the interlayer space of SAP,
 627 which stabilizes the red color of flavylum cations. While adsorption in the
 628 CTAB_SAP-RG sample probably induced stabilization of the RG quinoidal base,
 629 leading to a blue color for the hybrid. The color for β -CD_SAP-RG is close to the one
 630 observed in SAP-RG and corroborates with the proposal of intercalation of the RG
 631 molecules in hybrids. Finally, the color for β -CD+CTAB_SAP-RG was between the
 632 colors of β -CD_SAP-RG and CTAB_SAP-RG, which is suggestive of a minor
 633 stabilization of RG quinoidal base than in CTAB_SAP-RG.

634

635 The ΔE^* value is related to total color difference and is indicative of the light
 636 stability of the pigments. Under air (Fig. 12A), the ΔE^* values of the pigments
 increased gradually with the increase of the ageing time. Finally, the values reached

637 10.5±0.9 for SAP-RG, 13.6±0.6 for β-CD_SAP-RG, 18.7±0.2 for β-CD+CTAB_SAP-
 638 RG and 19.3±2.5 for CTAB_SAP-RG after 192 h of light exposure. Lower ΔE*
 639 variation in SAP-RG and β-CD_SAP-RG under air is probably due to the protection of
 640 the dye in the interlayer space of the saponite creating an oxygen hindering and
 641 stabilizing the pigments under irradiation. Under nitrogen atmosphere, ΔE* values
 642 were lower after 192 h of light exposure, the ΔE* values were 2.7±0.2, 3.3±0.2, 4.8±0.5
 643 and 5.7±0.9 for CTAB_SAP-RG, SAP-RG, β-CD+CTAB_SAP-RG and β-CD_SAP-
 644 RG, respectively. In addition, when the photostabilities under air are compared to
 645 photostabilities under nitrogen, the most significant differences were observed for β-
 646 CD+CTAB_SAP-RG and CTAB_SAP-RG, which corroborate with the greater
 647 exposure of RG molecules to oxygen attack on air atmosphere for these hybrids. The
 648 ΔE* values are summarized in Table 4.

649

650 **Table 4.** Total color differences (ΔE*) for each sample after 192 h of light exposure
 651 under air and nitrogen atmosphere.

Sample	ΔE* in air	ΔE* in N ₂
SAP-RG	10.5±0.9	3.3±0.2
CTAB_SAP-RG	19.3±2.5	2.7±0.2
β-CD_SAP-RG	13.6±0.6	5.7±0.9
β-CD+CTAB_SAP-RG	18.7±0.2	4.8±0.5

652

653 4 Conclusion

654

655 Hybrid pigments were successfully prepared by incorporating anthocyanin into
 656 unmodified and modified clay mineral based on synthetic SAP and CTAB and β-CD.

657 The hybrid pigments exhibit different colors function of their host-guest
 658 interactions. The presence of the quinoidal base form of anthocyanin molecule in
 659 CTAB_SAP-RG sample is probably more pronounced than in the other hybrids, which
 660 explains their initial blue color. The enhanced stability against visible light irradiation
 661 and basic environment conditions were brought by the electrostatic interaction between
 662 the dye and the respective host materials. The intercalation of the dye molecules into the
 663 interlayer spaces of saponite in β-CD_SAP-RG and SAP-RG protect the dyes from
 664 oxygen avoiding oxidation or the formation of other possible reactive oxygen species.
 665 **Reversibility in color upon exposure to acidic and basic atmosphere** is an evidence for a

666 possible application of the obtained pigments as a sensor to atmospheric acidity, which
667 can be exploited in several cycles if applied in less extreme pH conditions. These dyed
668 materials are environmentally friendly and can be promising candidates in different
669 application fields

670

671 **Acknowledgments**

672

673 We acknowledge the financial support from the CAPES/COFEBUB (Project n°
674 835/15), CAPES and National Council for Scientific and Technological Development
675 (CNPq, Brazil) for financial support (Grant [310921/2017-1](#), [M.G.F. 307460/2016-9](#),
676 [E.C.S.F.](#)). The authors thank the Île-de-France region and CNRS for funding.

677

678 **References**

679

- 680 [1] G. Zhuang, F. Rodrigues, Z. Zhang, M.G. Fonseca, P. Walter, M. Jaber, Dressing
681 protective clothing: stabilizing alizarin/halloysite hybrid pigment and beyond,
682 Dye. Pigment. 166 (2019) 32–41. <https://doi.org/10.1016/j.dyepig.2019.03.006>.
- 683 [2] A.F. Vinha, F. Rodrigues, M.A. Nunes, M.B.P.P. Oliveira, Natural pigments and
684 colorants in foods and beverages, Elsevier Inc., 2018.
685 <https://doi.org/10.1016/B978-0-12-813572-3.00011-7>.
- 686 [3] K. Marszałek, Ł. Woźniak, B. Kruszewski, S. Skapska, The effect of high
687 pressure techniques on the stability of anthocyanins in fruit and vegetables, Int. J.
688 Mol. Sci. 18 (2017). <https://doi.org/10.3390/ijms18020277>.
- 689 [4] I. Fatimah, D. Rubiyanto, N.I. Prakoso, A. Yahya, Y.-L. Sim, Green conversion
690 of citral and citronellal using tris(bipyridine)ruthenium(II)-supported saponite
691 catalyst under microwave irradiation, Sustain. Chem. Pharm. 11 (2019) 61–70.
692 <https://doi.org/10.1016/J.SCP.2019.01.001>.
- 693 [5] T.J. Lopes, M.G.N. Quadri, M.B. Quadri, Recovery of anthocyanins from red
694 cabbage using sandy porous medium enriched with clay, Appl. Clay Sci. 37
695 (2007) 97–106. <https://doi.org/10.1016/j.clay.2006.11.003>.
- 696 [6] H.L. Ribeiro, E.S. Brito, M. de sá M. Souza Filho, H.M.C. Azeredo,
697 Montmorillonite as a reinforcement and color stabilizer of gelatin films
698 containing acerola juice, Appl. Clay Sci. 165 (2018) 1–7.
699 <https://doi.org/10.1016/j.clay.2018.07.041>.

- 700 [7] E. Lima, P. Bosch, S. Loera, I.A. Ibarra, H. Laguna, V. Lara, Non-toxic hybrid
701 pigments: Sequestering betanidin chromophores on inorganic matrices, *Appl.*
702 *Clay Sci.* 42 (2009) 478–482. <https://doi.org/10.1016/j.clay.2008.06.005>.
- 703 [8] J.-L. Fang, Y. Luo, K. Yuan, Y. Guo, S.-H. Jin, Preparation and evaluation of an
704 encapsulated anthocyanin complex for enhancing the stability of anthocyanin,
705 *LWT - Food Sci. Technol.* 117 (2020) 1–8.
706 <https://doi.org/10.1016/J.LWT.2019.108543>.
- 707 [9] R. Brouillard, Chemical Structure of Anthocyanins, in: P. Markakis (Ed.),
708 *Anthocyanins As Food Color.*, Academic Press, 1982: pp. 1–40.
709 <https://doi.org/10.1016/b978-0-12-472550-8.50005-6>.
- 710 [10] B. Torres, B.K. Tiwari, A. Patras, P.J. Cullen, N. Brunton, C.P. O'Donnell,
711 Stability of anthocyanins and ascorbic acid of high pressure processed blood
712 orange juice during storage, *Innov. Food Sci. Emerg. Technol.* 12 (2011) 93–97.
713 <https://doi.org/10.1016/J.IFSET.2011.01.005>.
- 714 [11] B. Piffaut, F. Kader, M. Girardin, M. Metche, Comparative degradation pathways
715 of malvidin 3,5-diglucoside after enzymatic and thermal treatments, *Food Chem.*
716 50 (1994) 115–120. [https://doi.org/10.1016/0308-8146\(94\)90106-6](https://doi.org/10.1016/0308-8146(94)90106-6).
- 717 [12] Y. Kohno, R. Kinoshita, S. Ikoma, K. Yoda, M. Shibata, R. Matsushima, Y.
718 Tomita, Y. Maeda, K. Kobayashi, Stabilization of natural anthocyanin by
719 intercalation into montmorillonite, *Appl. Clay Sci.* 42 (2009) 519–523.
720 <https://doi.org/10.1016/j.clay.2008.06.012>.
- 721 [13] P. Pimchan, N. Khaorapapong, M. Ogawa, The effect of
722 cetyltrimethylammonium ion and type of smectites on the luminescence
723 efficiency of bis(8-hydroxyquinoline)zinc(II) complex, *Appl. Clay Sci.* 101
724 (2014) 223–228. <https://doi.org/10.1016/J.CLAY.2014.08.004>.
- 725 [14] Â.A. Teixeira-Neto, C.M.S. Izumi, M.L.A. Temperini, A.M.D.C. Ferreira,
726 V.R.L. Constantino, Hybrid materials based on smectite clays and nutraceutical
727 anthocyanins from the Açai fruit, *Eur. J. Inorg. Chem.* (2012) 5411–5420.
728 <https://doi.org/10.1002/ejic.201200702>.
- 729 [15] G. Zhuang, M. Jaber, F. Rodrigues, B. Rigaud, P. Walter, Z. Zhang, A new
730 durable pigment with hydrophobic surface based on natural nanotubes and
731 indigo: Interactions and stability, *J. Colloid Interface Sci.* 552 (2019) 204–217.
732 <https://doi.org/10.1016/J.JCIS.2019.04.072>.
- 733 [16] P. Trigueiro, F.A.R. Pereira, D. Guillermin, B. Rigaud, S. Balme, J.M. Janot,

734 I.M.G. dos Santos, M.G. Fonseca, P. Walter, M. Jaber, When anthraquinone dyes
735 meet pillared montmorillonite: Stability or fading upon exposure to light?, *Dye.*
736 *Pigment.* 159 (2018) 384–394. <https://doi.org/10.1016/j.dyepig.2018.06.046>.

737 [17] H.L. Ribeiro, A.V. de Oliveira, E.S. d. Brito, P.R.V. Ribeiro, M. de sá M. Souza
738 Filho, H.M.C. Azeredo, Stabilizing effect of montmorillonite on acerola juice
739 anthocyanins, *Food Chem.* 245 (2018) 966–973.
740 <https://doi.org/10.1016/j.foodchem.2017.11.076>.

741 [18] S.M. Eskandarabadi, M. Mahmoudian, K.R. Farah, A. Abdali, E. Nozad, M.
742 Enayati, Active intelligent packaging film based on ethylene vinyl acetate
743 nanocomposite containing extracted anthocyanin, rosemary extract and ZnO/Fe-
744 MMT nanoparticles, *Food Packag. Shelf Life.* 22 (2019) 100389.
745 <https://doi.org/10.1016/j.fpsl.2019.100389>.

746 [19] S. Li, J. Ding, B. Mu, X. Wang, Y. Kang, A. Wang, Acid/base reversible
747 allochroic anthocyanin/palygorskite hybrid pigments: Preparation, stability and
748 potential applications, *Dye. Pigment.* 171 (2019) 107738.
749 <https://doi.org/10.1016/J.DYEPIG.2019.107738>.

750 [20] G.T.M. Silva, C.P. Silva, M.H. Gehlen, J. Oake, C. Bohne, F.H. Quina,
751 Organic/inorganic hybrid pigments from flavylum cations and palygorskite,
752 *Appl. Clay Sci.* 162 (2018) 478–486. <https://doi.org/10.1016/j.clay.2018.07.002>.

753 [21] G.T.M. Silva, K.M. Da Silva, C.P. Silva, A.C.B. Rodrigues, J. Oake, M.H.
754 Gehlen, C. Bohne, F.H. Quina, Highly fluorescent hybrid pigments from
755 anthocyanin- and red wine pyranoanthocyanin-analogs adsorbed on sepiolite
756 clay, *Photochem. Photobiol. Sci.* 18 (2019) 1750–1760.
757 <https://doi.org/10.1039/c9pp00141g>.

758 [22] C. Capello, G.C. Leandro, C.E. Maduro Campos, D. Hotza, B.A. Mattar Carciofi,
759 G.A. Valencia, Adsorption and desorption of eggplant peel anthocyanins on a
760 synthetic layered silicate, *J. Food Eng.* 262 (2019) 162–169.
761 <https://doi.org/10.1016/J.JFOODENG.2019.06.010>.

762 [23] M. Ogawa, R. Takee, Y. Okabe, Y. Seki, Bio-geo hybrid pigment; clay-
763 anthocyanin complex which changes color depending on the atmosphere, *Dye.*
764 *Pigment.* 139 (2017) 561–565. <https://doi.org/10.1016/J.DYEPIG.2016.12.054>.

765 [24] C. Zhang, H. He, Q. Tao, S. Ji, S. Li, L. Ma, X. Su, J. Zhu, Metal occupancy and
766 its influence on thermal stability of synthetic saponites, *Appl. Clay Sci.* 135
767 (2017) 282–288. <https://doi.org/10.1016/J.CLAY.2016.10.006>.

- 768 [25] C.H. Zhou, Q. Zhou, Q.Q. Wu, S. Petit, X.C. Jiang, S.T. Xia, C.S. Li, W.H. Yu,
769 Modification, hybridization and applications of saponite: An overview, *Appl.*
770 *Clay Sci.* 168 (2019) 136–154. <https://doi.org/10.1016/J.CLAY.2018.11.002>.
- 771 [26] M. Jaber, J. Miéché-Brendlé, Influence du milieu de synthèse sur la cristallisation
772 de saponite: Proposition de mécanisme réactionnel en milieux acide et basique,
773 *Comptes Rendus Chim.* 8 (2005) 229–234.
774 <https://doi.org/10.1016/j.crci.2004.10.025>.
- 775 [27] V. Tangaraj, J.-M. Janot, M. Jaber, M. Bechelany, S. Balme, Adsorption and
776 photophysical properties of fluorescent dyes over montmorillonite and saponite
777 modified by surfactant, *Chemosphere.* 184 (2017) 1355–1361.
778 <https://doi.org/10.1016/J.CHEMOSPHERE.2017.06.126>.
- 779 [28] M. Polverejan, Y. Liu an, T. J.Pinnavaia, Mesostructured clay catalysts: a new
780 porous clay heterostructure (PCH) derived from synthetic saponite, *Stud. Surf.*
781 *Sci. Catal.* 129 (2000) 401–408. [https://doi.org/10.1016/S0167-2991\(00\)80239-6](https://doi.org/10.1016/S0167-2991(00)80239-6).
- 782 [29] H. Han, M.K. Rafiq, T. Zhou, R. Xu, O. Mašek, X. Li, A critical review of clay-
783 based composites with enhanced adsorption performance for metal and organic
784 pollutants, *J. Hazard. Mater.* 369 (2019) 780–796.
785 <https://doi.org/10.1016/J.JHAZMAT.2019.02.003>.
- 786 [30] F. Bergaya, M. Jaber, J. Lambert, Organophilic clay minerals, in: M. Galimberti
787 (Ed.), *Rubber Clay Nanocomposites. Sci. Technol. Appl., First Edit*, J. Wiley &
788 sons, 2011: pp. 45–86. <https://doi.org/10.1002/9781118092866.ch2>.
- 789 [31] V. Lozano-Morales, I. Gardi, S. Nir, T. Undabeytia, Removal of pharmaceuticals
790 from water by clay-cationic starch sorbents, *J. Clean. Prod.* 190 (2018) 703–711.
791 <https://doi.org/10.1016/J.JCLEPRO.2018.04.174>.
- 792 [32] M. Koosha, S. Hamedí, Intelligent Chitosan/PVA nanocomposite films
793 containing black carrot anthocyanin and bentonite nanoclays with improved
794 mechanical, thermal and antibacterial properties, *Prog. Org. Coatings.* 127 (2019)
795 338–347. <https://doi.org/10.1016/J.PORGCOAT.2018.11.028>.
- 796 [33] E. Abu-Danso, S. Peräniemi, T. Leiviskä, T. Kim, K.M. Tripathi, A. Bhatnagar,
797 Synthesis of clay-cellulose biocomposite for the removal of toxic metal ions from
798 aqueous medium, *J. Hazard. Mater.* 381 (2020) 120871.
799 <https://doi.org/10.1016/J.JHAZMAT.2019.120871>.
- 800 [34] P. Mura, F. Maestrelli, C. Aguzzi, C. Viseras, Hybrid systems based on “drug –
801 in cyclodextrin – in nanoclays” for improving oxaprozin dissolution properties,

- 802 Int. J. Pharm. 509 (2016) 8–15. <https://doi.org/10.1016/J.IJPHARM.2016.05.028>.
- 803 [35] I. Mourtzinou, D.P. Makris, K. Yannakopoulou, N. Kalogeropoulos, I. Michali,
804 V.T. Karathanos, Thermal stability of anthocyanin extract of *Hibiscus sabdariffa*
805 L. in the presence of β -cyclodextrin, *J. Agric. Food Chem.* 56 (2008) 10303–
806 10310. <https://doi.org/10.1021/jf801389j>.
- 807 [36] M. Buchweitz, M. Speth, D.R. Kammerer, R. Carle, Impact of pectin type on the
808 storage stability of black currant (*Ribes nigrum* L.) anthocyanins in pectic model
809 solutions, *Food Chem.* 139 (2013) 1168–1178.
810 <https://doi.org/10.1016/J.FOODCHEM.2013.02.005>.
- 811 [37] C.C. Rusa, C. Luca, A.E. Tonelli, Polymer-cyclodextrin inclusion compounds:
812 Toward new aspects of their inclusion mechanism, *Macromolecules.* 34 (2001)
813 1318–1322. <https://doi.org/10.1021/ma001868c>.
- 814 [38] A. Bagheri, A.A. Rafati, Thermodynamic investigation of inclusion complex
815 formation between cetyltrimethyl ammonium bromide (CTAB) and β -
816 cyclodextrin at various temperatures, *J. Mol. Liq.* 195 (2014) 145–149.
817 <https://doi.org/10.1016/J.MOLLIQ.2014.02.020>.
- 818 [39] D.-R. Yei, S.-W. Kuo, H.-K. Fu, F.-C. Chang, Enhanced thermal properties of PS
819 nanocomposites formed from montmorillonite treated with a
820 surfactant/cyclodextrin inclusion complex, *Polymer (Guildf).* 46 (2005) 741–750.
821 <https://doi.org/10.1016/J.POLYMER.2004.11.108>.
- 822 [40] S. Lagergren, Zurtheorie der sogenannten adsorption gelosterstoffe, *K. Vet.*
823 *Akad. Handl.* 24 (1898) 1–39.
- 824 [41] Y.. Ho, G. McKay, Pseudo-second order model for sorption processes, *Process*
825 *Biochem.* 34 (1999) 451–465. [https://doi.org/10.1016/S0032-9592\(98\)00112-5](https://doi.org/10.1016/S0032-9592(98)00112-5).
- 826 [42] S.Y. Elovich, L. G., Theory of adsorption from solutions of non electrolytes on
827 solid (I) equation adsorption from solutions and the analysis of its simplest form,
828 (ii) verification of the equation of adsorption isotherm from solutions, *Izv. Sib.*
829 *Otd. An. Khim.* 2 (1962) 209–216.
- 830 [43] I. Langmuir, The adsorption of gases on plane surfaces of glass, mica and
831 platinum, *J. Am. Chem. Soc.* 40 (1918) 1361–1403.
832 <https://doi.org/10.1021/ja02242a004>.
- 833 [44] H. Freundlich, Über die Adsorption in Lösungen, *Zeitschrift Für Phys. Chemie.*
834 *57U* (1907). <https://doi.org/10.1515/zpch-1907-5723>.
- 835 [45] M.J. Temkin, V. Pyzhev, Recent modifications to Langmuir isotherms, *Acta*

- 836 Phys. Chim. 12 (1940) 217–222.
- 837 [46] G.T.M. Silva, C.P. Silva, M.H. Gehlen, J. Oake, C. Bohne, F.H. Quina,
838 Organic/inorganic hybrid pigments from flavylum cations and palygorskite,
839 Appl. Clay Sci. 162 (2018) 478–486. <https://doi.org/10.1016/j.clay.2018.07.002>.
- 840 [47] M. Kundu, S. Saha, M.N. Roy, Evidences for complexations of β -cyclodextrin
841 with some amino acids by ^1H NMR, surface tension, volumetric investigations
842 and XRD, J. Mol. Liq. 240 (2017) 570–577.
843 <https://doi.org/10.1016/J.MOLLIQ.2017.05.123>.
- 844 [48] S. Gao, Y. Liu, J. Jiang, Q. Ji, Y. Fu, L. Zhao, C. Li, F. Ye, Physicochemical
845 properties and fungicidal activity of inclusion complexes of fungicide
846 chlorothalonil with β -cyclodextrin and hydroxypropyl- β -cyclodextrin, J. Mol.
847 Liq. 293 (2019) 111513. <https://doi.org/10.1016/J.MOLLIQ.2019.111513>.
- 848 [49] K. El Adraa, V. Timon, J.F. Lambert, A.R. Al-Rabaa, F. Jaber, M. Jaber, F.
849 Tielens, Adsorption of l-DOPA intercalated in hydrated Na-saponite clay: A
850 combined experimental and theoretical study, J. Phys. Chem. C. 116 (2012)
851 26414–26421. <https://doi.org/10.1021/jp3094148>.
- 852 [50] L. Marçal, E.H. De Faria, E.J. Nassar, R. Trujillano, N. Martín, M.A. Vicente, V.
853 Rives, A. Gil, S.A. Korili, K.J. Ciuffi, Organically Modified Saponites: SAXS
854 Study of Swelling and Application in Caffeine Removal, ACS Appl. Mater.
855 Interfaces. 7 (2015) 10853–10862. <https://doi.org/10.1021/acsami.5b01894>.
- 856 [51] N. Li, L. Xu, Thermal analysis of β -cyclodextrin/Berberine chloride inclusion
857 compounds, Thermochim. Acta. 499 (2010) 166–170.
858 <https://doi.org/10.1016/j.tca.2009.10.014>.
- 859 [52] A.M. dos Santos Moreira, V.C.E. Bittencourt, F.L.S. Costa, M. Elena de Lima,
860 M.T.P. Lopes, W.S. Borges, G.F. Martins, C.S. Nascimento, J.G. da Silva,
861 Â.M.L. Denadai, K.B. Borges, Hydrophobic Nanoprecipitates of β -
862 Cyclodextrin/Avermectins Inclusion Compounds Reveal Insecticide Activity
863 against *Aedes aegypti* Larvae and Low Toxicity against Fibroblasts, J. Agric.
864 Food Chem. 66 (2018) 7275–7285. <https://doi.org/10.1021/acs.jafc.8b01300>.
- 865 [53] A.F. Cortez Campos, P.H. Michels-Brito, F.G. da Silva, R.C. Gomes, G. Gomide,
866 J. Depeyrot, Removal of direct yellow 12 from water using CTAB-coated core-
867 shell bimagnetic nanoadsorbents, J. Environ. Chem. Eng. (2019) 103031.
868 <https://doi.org/10.1016/J.JECE.2019.103031>.
- 869 [54] M. Mobarak, A.Q. Selim, E.A. Mohamed, M.K. Seliem, A superior adsorbent of

870 CTAB/H₂O₂ solution–modified organic carbon rich-clay for hexavalent
871 chromium and methyl orange uptake from solutions, *J. Mol. Liq.* 259 (2018)
872 384–397. <https://doi.org/10.1016/J.MOLLIQ.2018.02.014>.

873 [55] T.M. De Miranda, A.R. De Oliveira, J.R. Pereira, J.G. Da Silva, I.S. Lula, C.S.
874 Nascimento, Â.M. I. Denadai, Inclusion vs. micellization in the cetylpyridine
875 chloride / β -cyclodextrin system: A structural and thermodynamic approach, *J.*
876 *Mol. Struct.* 1184 (2019) 289–297. <https://doi.org/S0022286019301632>.

877 [56] Q. Tao, Y. Fang, T. Li, D. Zhang, M. Chen, S. Ji, H. He, S. Komarneni, H.
878 Zhang, Y. Dong, Y.D. Noh, Silylation of saponite with 3-
879 aminopropyltriethoxysilane, *Appl. Clay Sci.* 132–133 (2016) 133–139.
880 <https://doi.org/10.1016/J.CLAY.2016.05.026>.

881 [57] J. Madejová, Ľ. Jankovič, M. Slaný, V. Hronský, Conformation heterogeneity of
882 alkylammonium surfactants self-assembled on montmorillonite: Effect of head-
883 group structure and temperature, *Appl. Surf. Sci.* 503 (2020) 144125.
884 <https://doi.org/10.1016/j.apsusc.2019.144125>.

885 [58] S.J. Heyes, N.J. Clayden, M. Dobson, ¹³C-CP / MAS NMR studies of the
886 cyclomalto-oligosaccharide (cyclodextrin) hydrates, 233 (1992) 1–14.

887 [59] N. Saito, K. Toki, T. Honda, K. Kawase, Cyanidin 3-malonylglucuronide
888 in *Bellis* and cyanidin 3-malonylglucoside in *Dendranthema*, *Phytochemistry*. 27
889 (1988) 2963–2966. [https://doi.org/10.1016/0031-9422\(88\)80697-6](https://doi.org/10.1016/0031-9422(88)80697-6).

890 [60] M. Wolniak, I. Wawer, ¹³C CPMAS NMR and DFT calculations of
891 anthocyanidins, *Solid State Nucl. Magn. Reson.* 34 (2008) 44–51.
892 <https://doi.org/10.1016/j.ssnmr.2008.06.003>.

893 [61] I. Chaari, E. Fakhfakh, M. Medhioub, F. Jamoussi, Comparative study on
894 adsorption of cationic and anionic dyes by smectite rich natural clays, *J. Mol.*
895 *Struct.* 1179 (2019) 672–677.
896 <https://doi.org/10.1016/J.MOLSTRUC.2018.11.039>.

897 [62] D.F. Brito, E.C. da Silva Filho, M.G. Fonseca, M. Jaber, Organophilic bentonites
898 obtained by microwave heating as adsorbents for anionic dyes, *J. Environ. Chem.*
899 *Eng.* 6 (2018) 7080–7090. <https://doi.org/10.1016/J.JECE.2018.11.006>.

900 [63] F. De Castro Silva, M.M.F. Da Silva, L.C.B. Lima, J.A. Osajima, E.C. Da Silva
901 Filho, Integrating chloroethyl phosphate with biopolymer cellulose and assessing
902 their potential for absorbing brilliant green dye, *J. Environ. Chem. Eng.* 4 (2016).
903 <https://doi.org/10.1016/j.jece.2016.07.010>.

- 904 [64] S. Gamoudi, E. Srasra, Adsorption of organic dyes by HDPy⁺-modified clay:
905 Effect of molecular structure on the adsorption, *J. Mol. Struct.* 1193 (2019) 522–
906 531. <https://doi.org/10.1016/J.MOLSTRUC.2019.05.055>.
- 907 [65] N. Belhouchat, H. Zaghouane-Boudiaf, C. Viseras, Removal of anionic and
908 cationic dyes from aqueous solution with activated organo-bentonite/sodium
909 alginate encapsulated beads, *Appl. Clay Sci.* 135 (2017) 9–15.
910 <https://doi.org/10.1016/J.CLAY.2016.08.031>.
- 911 [66] C. Tan, G.B. Celli, M.J. Selig, A. Abbaspourrad, Catechin modulates the
912 copigmentation and encapsulation of anthocyanins in polyelectrolyte complexes
913 (PECs) for natural colorant stabilization, *Food Chem.* 264 (2018) 342–349.
914 <https://doi.org/10.1016/J.FOODCHEM.2018.05.018>.
- 915